nature communications

Article

https://doi.org/10.1038/s41467-025-57404-6

E3 ubiquitin ligase RNF128 promotes Lys63-linked polyubiquitination on SRB1 in macrophages and aggravates atherosclerosis

Received: 4 November 2023

Accepted: 20 February 2025

Published online: 04 March 2025

Check for updates

Yapeng Liu[1], Xinyu Zhang[1], Liwen Yu[1], Lei Cao[1], Jie Zhang[1], Qian Li[1], Xiaohong Wang[1], Wenqian Qi[1], Liangyu Cai[1], Ruiqing Ren[1], Weiwei Wang[1], Xiaobin Guo[2], Guohai Su[2], Bo Xi[3], Yun Zhang[1,2], Chengjiang Gao[4] ✉, Meng Zhang[1,2] ✉ & Cheng Zhang[1,2] ✉

Macrophage-derived foam cell formation is the hallmark of atherosclerotic plaques prominently attributed to excessive lipid uptake and metabolic disorders. As a classic membrane-localized ubiquitin ligase, the role of RNF128 in atherosclerosis remains unknown. We discover that RNF128 is specifically expressed in macrophages of the lipid core based on single-cell RNA sequencing data and persistent hyperlipidemia induces the high expression of RNF128 in macrophages. RNF128 ablation in macrophages ameliorates atherosclerosis in both male and female mice under the background of ApoE and LDLR deficiency. Mechanistically, RNF128 directly binds to scavenger receptor B1 (SRB1), preventing its degradation through the lysosomal system and promoting oxidized low-density lipoprotein (oxLDL)-induced foam cell formation and inflammatory response in macrophages. In addition, RNF128 catalyzes Lys63-linked polyubiquitination on the cytoplasmic C-terminus of the SRB1 at lysine 478, which promotes the endosome SRB1 recycling to the cell membrane with the assistance of Rab11, instead of entering the lysosome for degradation.

Atherosclerosis develops silently with the narrowing of arteries due to atheroma formation initiated by maladaptive accumulation of cholesterol and chronic inflammation[1,2]. Lipid metabolic disturbance drives hyperlipidemia that promotes plaque progression. Despite the advance in its management, atherosclerotic cardiovascular disease accounts for most mortality worldwide, urging new therapeutic targets to combat this destructive disease[3–6]. The conversion of plaque macrophages to foam cells is an essential mechanism by which lipids promote atherogenesis[7]. Cholesterol-engorged and proinflammatory macrophage-derived foam cells exert a prominent role in all phases of the plaque's life cycle[8–10]. Macrophage scavenger receptors, including scavenger receptor A1 (SRA1), SRB1 (encoded by *Scarb1* or *SCARB1*), and cluster determinant 36 (CD36), are characterized by their ability to recognize and internalize native cholesterol-rich low-density lipoprotein (LDL) or modified LDL such as oxidized LDL (oxLDL)[11,12]. Macrophage ATP-binding cassette (ABC) transporters ABCA1 and ABCG1 facilitate the outflow of excess cholesterol from the cells[11]. Either unwarranted influx of lipid or disturbed cholesterol efflux stimulates atherogenesis[13,14]. Thus, further insight into the mechanisms that avoid lipid retention in macrophages can serve new therapeutic opportunities.

[1]State Key Laboratory for Innovation and Transformation of Luobing Theory; Key Laboratory of Cardiovascular Remodeling and Function Research of MOE, NHC, CAMS and Shandong Province; Department of Cardiology, Qilu Hospital of Shandong University, Jinan, China. [2]Cardiovascular Disease Research Center of Shandong First Medical University, Central Hospital Affiliated to Shandong First Medical University, Jinan, China. [3]Department of Epidemiology, School of Public Health, Cheeloo College of Medicine, Shandong University, Jinan, China. [4]Shandong Key Laboratory of Infection and Immunity, Department of Immunology, School of Basic Medical Sciences, Shandong University, Jinan, China. ✉e-mail: cgao@sdu.edu.cn; zhangmeng@sdu.edu.cn; zhangc@sdu.edu.cn

SRB1 belongs to the class B scavenger receptor family, and shares a remarkably similar protein structure with CD36 and LIMP2[15]. Therefore, SRB1 exhibits the same ligand-binding interface and similar functional properties with CD36 to bind with oxLDL and high-density lipoprotein (HDL) for uptake. SRB1 involves in the selective uptake of HDL in hepatocytes and the promotion of reverse cholesterol transport (RCT) in the liver[14,15], and SRB1 is also reported to recognize oxLDL with greater binding activity than HDL, native LDL, and acetylated LDL (acLDL), triggering the resultant internalization and degradation of oxLDL[16]. Huang et al. has demonstrated a pro-atherogenic role of SRB1 by promoting native and modified LDL transcytosis in endothelial cells[17,18], indicating that the function of SRB1 in other cell types may be different to that in hepatocytes. In macrophages, SRB1 can, in principle, function as an oxLDL scavenger receptor for the uptake and degradation of oxidized lipoproteins in vitro[16,19] while it slightly contributes to efflux[16,20].

Endocytosis involving scavenger receptors plays vital and initial roles in atherosclerosis[16,21]. SRB1 could mediate the internalization and degradation of oxLDL through the endocytic pathway, and is further recycled to the cell membrane for a new round of internalization[13]. At the same time, SRB1 on the cell surface and inside the cell may play coordinated but distinct roles in different stages of lipid endocytosis and degradation, and foam cells will be formed when there is more lipid endocytosis than lipid clearance, especially in a state of persistent excess hyperlipidemia[16,22]. Up to now, the roles of SRB1 in macrophages remain controversial, and the regulatory mechanisms of macrophage SRB1 on oxLDL endocytosis need to be explored in deep.

Notably, SRB1 can be degraded post-transcriptionally via ubiquitin signaling[23], whose specific explication remains lacking. Therefore, whether and how ubiquitylation regulates oxLDL endocytosis via SRB1 requires investigation. Ubiquitination is indispensable in the endocytosis of membrane proteins[24]. Ubiquitin ligase E3 regulates the progression of atherosclerosis through several aspects, including promoting protein ubiquitination to alter cholesterol uptake and modulating inflammation during atherogenesis[25,26]. The ubiquitin E3 ligase RNF128 (or GRAIL) has been characterized as a single transmembrane protein containing a cytosolic RING domain, localizing to the endosomal recycling pathway, different from other E3 ligases[27]. RNF128 targets membrane-associated molecules (including CD83 and CD40L) for regulating cellular events, predominantly in $CD4^+$ T-cell anergy[28], innate antiviral immunity[29], and progression of Barrett's esophagus[30], hepatic steatosis[31], and diet-induced obesity[32]. However, the involvement of RNF128 in atherogenesis is unclear.

In this study, we revealed the unsuspected RNF128 role in foam cell formation and its positive correlation with atherosclerosis in both mice and humans. Mice with macrophage-specific RNF128 conditional knockout ($RNF128^{fl/fl}Lyz2^{cre}$) on an apolipoprotein E null ($ApoE^{-/-}$) background ameliorated the development of atherosclerosis in both males and females, which was phenocopied in LDL receptor (LDLR)-deficient mice induced by PCSK9. Mechanistically, the direct interaction between RNF128 and SRB1 was first discovered, and RNF128 promoted Lys63 (K63)-ubiquitination of SRB1 at the lysine 478 site, which promoted Rab11-mediated recycling to the membrane and facilitated oxLDL endocytic process. Consequently, macrophages suffered from accumulated lipid and augmented inflammation to be present as foam cells. Thus, proper intervention of macrophage-RNF128 creates a meaningful therapeutic potential.

Results

RNF128 expression in macrophages is augmented during the development of atherosclerosis

We obtained the single-cell RNA sequencing (scRNA-seq) data using the Chromium Single Cell Gene Expression system (10 × Genomics, Pleasanton, CA, USA) from atherosclerotic plaques of $Ldlr^{-/-}$ mice fed a Western diet (WD) for 0, 8, 16, and 26 weeks[33]. Cells were annotated into 9 clusters in t-SNE (t-distributed stochastic neighbor embedding) visualization: vascular smooth muscle cell (VSMC), T cell, granulocyte (Granu), endothelial cell (EC), fibroblast (Fibro), neuron cell, monocyte (Mono), dendritic cell (DC), and macrophage (Macro), among which macrophages were clustered with robust expression of *Lyz2* and *Cd68* (Fig. 1A and S1a). Further analysis revealed that the *Rnf128* expression almost exclusively existed in macrophages compared to their low expression in other cell types, including monocytes and granulocytes (Fig. 1B and S1b). Moreover, *Rnf128* overlapped satisfactorily with the macrophage marker, *Lyz2*, with a high colocalization rate, representing a population of $Rnf128^{+}Lyz2^{hi}$ macrophages (Fig. 1C and S1c). After WD, the number of *Rnf128*-expressing macrophages increased, and a considerably increased number of $Rnf128^{+}Lyz2^{hi}$ macrophages were also discovered in atheromatous plaques (Fig. 1D, E). The gene expression level of *Rnf128* colocalized with *Lyz2* was also augmented during atherosclerosis (Fig. S1d). Thus, we hypothesized that macrophage *Rnf128* might exhibit a critical role in atherosclerosis.

To determine the specific expression of RNF128 in macrophages, immunoflurescence staining for RNF128 and MOMA-2 (specific for monocytes and macrophages) was performed on plaques on the aortic root sections of mice, revealing that RNF128 could colocalize with MOMA-2 (Fig. S1e), but not α-SMA (α-smooth muscle actin) (Fig. S1f) and CD31 (endothelial marker) (Fig. S1g). Then, an immunofluorescent assay for RNF128 and MOMA-2 was performed on the aortic root sections of $ApoE^{-/-}$ mice with WD feeding for various durations (8 and 20 weeks) to determine the RNF128 protein level within atherosclerotic lesions. RNF128 and MOMA-2 expression showed a significant colocalization in advanced lesions and early lesions. Compared with the early lesions, the protein level of RNF128 was upregulated (Fig. 1F and S2a). Additionally, the increase in RNF128 protein during processive lesions was further verified by Western blotting of whole-aorta lysates for RNF128 (Fig. 1G). Human coronary atheroma from early and advanced lesions was stained with RNF128 and MOMA-2 antibodies to confirm the clinical significance of RNF128. According to the American Heart Association classification, early lesions are characterized by fatty dots or streak while calcified and fibrous plaques would be found in advanced lesions[34]. The intensity of RNF128 in the MOMA-2 positive region was markedly increased in the advanced lesions (Fig. 1H and S2b), consistent with the result observed in mice (Fig. 1F and S2a).

Besides, primary peritoneal macrophages (hereafter macrophages) from wild-type (WT) mice were isolated and incubated with oxLDL (75 μg/mL) for different time points (0, 6, 12, and 24 h). Immunofluorescence staining revealed that the RNF128 protein level was upregulated after oxLDL stimulation (Fig. 1I and S2c). The mRNA and protein expression of RNF128 increased in a time- and concentration-dependent manner in macrophages (Fig. 1J and S2d for time-dependence, 1k and S2e for concentration-dependence). Furthermore, the time-dependent upregulation was confirmed in mouse macrophage cell line RAW264.7 (Fig. 1L and S2f) and human THP-1-derived macrophages (Fig. 1M and S2g). As both the inflammation and lipid accumulation could induce atherosclerosis, we treated macrophages with inflammatory inductors, including IL1β, IL6, and TNFα. However, the mRNA expression level of RNF128 were unchanged (Fig. S2h–j), indicating that RNF128 expression is mainly driven by lipid accumulation.

Macrophage-specific deletion of RNF128 attenuates foam cell formation by reducing lipid uptake

Because macrophage-derived foam cells act as a hallmark in all stages of atherosclerosis[35], we hypothesized that RNF128 might modulate lipid homeostasis in macrophages. First, we silenced the *RNF128* gene in macrophages from WT mice using small interfering RNA (siRNA). RNF128-deficient (RNF128-Si) macrophages exhibited a ~50% decrease in foam cell formation as demonstrated with Oil red O staining as well as neutral lipid dyed with boron-dipyrrolemethene (BODIPY) in the

https://doi.org/10.1038/s41467-025-57404-6

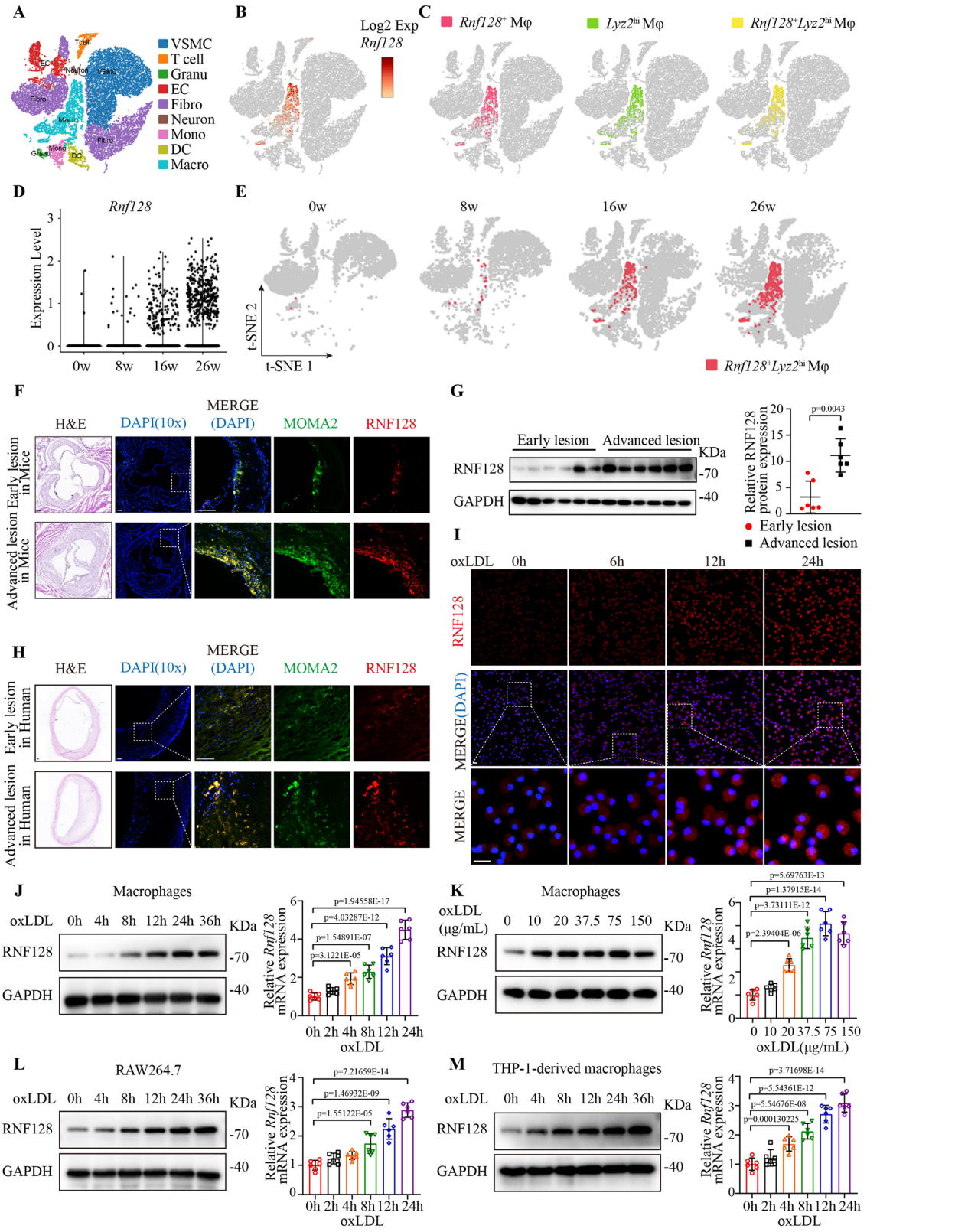

presence of oxLDL (Fig. S3a, b). Measurement of cellular total cholesterol indicated that macrophages with negative control (RNF128-NC) accumulated more cholesterol than RNF128-interfered cells (Fig. S3c).

To examine the functional importance of RNF128, mice with macrophage-specific conditional RNF128 knockout (RNF128-CKO) were generated (Fig. S3d), and $RNF128^{fl/fl}$ mice were used as controls (RNF128-WT). RNF128 expression was scarcely detectable at both mRNA and protein levels in primary peritoneal macrophages, confirming the selective elimination of RNF128 in macrophages (Fig. S3e, f). Similar results were observed in elicited peritoneal macrophages from $RNF128^{fl/fl}Lyz2^{cre}$ mice and its control group (Fig. 2A). To further prove the lipid-accumulation function of RNF128, RNF128 was overexpressed using adenovirus as a gene transfer carrying C-terminal

Fig. 1 | The expression of RNF128 in macrophages is augmented during atherogenesis. A Subset of cells from atherosclerotic aortas was annotated into nine clusters. **B** Location of cell clusters with *Rnf128* expression on the t-SNE plot. **C** Cell clusters with the expression of *Rnf128* (*Rnf128*$^{+}$Mφ, left), high expression of *Lyz2* (*Lyz2*^{hi}Mφ, middle), and both of these two genes (*Rnf128*$^{+}$*Lyz2*^{hi}Mφ, right). Mφ, macrophages. **D** The expression level of *Rnf128*-expressing macrophage numbers during the process of atherosclerosis. **E** The number of macrophages with high expression of *Rnf128* and *Lyz2* in atherosclerotic aortas of mice fed WD for different durations. **F** Colocalization analysis via immunofluorescence of RNF128 and MOMA-2 (specific for monocytes and macrophages) expression in early and advanced atherosclerotic lesions of apolipoprotein E null (ApoE$^{-/-}$) mice fed a WD for 8 weeks and 20 weeks, respectively ($n = 8$ per group, hereafter $n = 8$). Scale bar: 100 μm. **G** Western blotting images of RNF128 protein levels from whole aortas and quantitative analysis ($n = 6$). **H** Colocalization analysis of RNF128 and MOMA-2 expression in early and advanced atherosclerotic lesions from coronary atheromatous plaques of humans ($n = 8$). Scale bar: 100 μm. **I** Immunofluorescence of RNF128 in macrophages incubated with oxidized low-density lipoprotein (oxLDL, 75 μg/mL) for different time points ($n = 6$). Scale bar: 20 μm. **J** Western blotting (left, $n = 4$) and quantitative PCR (right, $n = 6$) of RNF128 expression in macrophages treated with oxLDL for different time points. **K** Western blotting (left, $n = 4$) and quantitative PCR (right, $n = 6$) of RNF128 expression in macrophages treated with a concentration gradient of oxLDL for 24 h. **L**, **M** Western blotting (left, $n = 4$) and quantitative PCR analysis (right, $n = 6$) of RNF128 expression in RAW264.7 and THP-1-derived macrophages treated with time-dependent oxLDL, respectively. The "*n*" represents the number of biologically independent samples. Data were presented as mean ± SD, Shapiro–Wilk method tested that all data were normally distributed. Unpaired two-tailed Student's *t*-test was used for (**G**). One-way ANOVA followed by the Dunnett post hoc test was used for the others. Adjusted *P* values were provided in case of multiple-group comparisons. Source data are provided as a Source Data file.

Flag-RNF128 (Flag-RNF128) and Flag-tagged vector (Flag-Vector) as the negative control. The overexpression of RNF128 facilitated lipid droplet accumulation in WT macrophages treated with oxLDL (Fig. 2B). Analogously, the total cholesterol content of macrophages was reduced by 46% in RNF128-invalidated cells after oxLDL treatment (Fig. 2C), consistent with the observation from BODIPY staining (Fig. 2D). The staining of lipid with BODIPY was also performed in macrophages with overexpressed RNF128, exhibiting a 1.5-fold increase compared to that in control cells (Fig. S3g).

Unrestrained uptake of lipoproteins and insufficient cholesterol efflux are responsible for foam cell formation[36]. Therefore, we examined whether RNF128 was involved in the increased lipid influx or inadequate cholesterol outflow. First, we performed an uptake assay of oxLDL labeled using a red fluorescent probe (Dil-oxLDL), which suggested that the fluorescence intensity of Dil-oxLDL was decreased in RNF128-silent macrophages compared with the control group (Fig. S3h). Subsequently, we treated the macrophages with native LDL (Dil-nLDL), whereas their fluorescence intensity was comparable between the two groups (Fig. S3i), indicating that RNF128 in macrophages might be essential for the internalization of modified LDL rather than native LDL. Similar findings were observed in macrophages isolated from RNF128$^{fl/fl}$Lyz2^{cre} mice (Fig. 2E) and macrophages with overexpressed RNF128 (Fig. 2F). Subsequently, we examined whether cholesterol efflux was also influenced by RNF128; however, no significant difference was observed when RNF128 was eliminated (Fig. 2G and S3j). Accordingly, macrophage-RNF128 fostered foam cell buildup by regulating lipid uptake.

The RING finger of RNF128 was established to exhibit E3 ligase activity. Mutation in the RING domain disturbed ubiquitin ligase activity[27]. Hence, we generated a catalytically inactive mutant of RNF128 lacking the RING domain based on the C-terminal Flag-RNF128 (Flag-RNF128 ΔR) to explore whether RNF128 modulated oxLDL uptake through E3 ligase activation. The RING deletion is relatively small so there was no detectable effect on migration of RNF128 protein (Fig. S3k). Overexpression of wild-type RNF128 (Flag-RNF128) rescued the diminished lipid accretion observed in RNF128$^{fl/fl}$Lyz2^{cre} macrophages, whereas overexpressed RNF128-mutant (Flag-RNF128 ΔR) lost this ability (Fig. 2H). For macrophages from RNF128$^{fl/fl}$ mice, Flag-RNF128 ΔR overexpression failed to facilitate lipid accumulation, achieved by Flag-RNF128 (Fig. 2H). In addition, RNF128 enhanced oxLDL uptake in a RING-dependent manner (Fig. 2I). Collectively, the macrophage-targeted absence of RNF128 attenuated oxLDL-induced lipid accumulation by reducing oxLDL uptake.

RNF128 deficiency downregulated SRB1 protein level and impacts foam cell formation

Based on the scRNA-seq data[33], Kyoto Encyclopedia of Genes and Genomes (KEGG) pathway enrichment was conducted, focusing subsequent analyses on *RNF128*$^{+}$*Lyz2*^{hi} macrophages. The top metabolic pathways were mainly enriched in the phagosome, lysosome, as well as lipid and atherosclerosis (Fig. 3A).

To investigate the exact target of RNF128 for modulating lipid homeostasis, we examined the expression of macrophage scavenger receptors contributing to foam cell development and ABCA1 and ABCG1 responsible for cholesterol outflow. For the mRNA description of SRB1, *Scarb1* is used instead of SRB1. SRB1 protein level was decreased in RNF128-interfered macrophages after oxLDL treatment, whereas no difference was observed in other receptors, ABCA1 and ABCG1 (Fig. S4a, b). Additionally, mRNA expression was unaffected by RNF128 deficiency in all groups (Fig. S4c), and a similar pattern was observed in macrophages derived from RNF128-CKO and RNF128-WT mice (Fig. 3B–D). In response to the stimulation of oxLDL, SRB1 declined at both mRNA and protein levels in macrophages, whereas RNF128 knockout further reduced the SRB1 protein expression after incubation with oxLDL for 12 and 24 h, respectively (Fig. 3C, D). However, SRB1 mRNA level was comparable between the two groups (Fig. 3B). Subsequently, we verified these findings through adenovirus-mediated RNF128 overexpression in macrophages, which was consistent with the effects of RNF128 loss-of-function (Fig. 3E and S5a, b). As a progressive and chronic inflammatory disease, atherosclerosis develops based on enhanced inflammation and lipid accumulation [12]. To investigate the role of RNF128 in the inflammatory response of macrophages, we treated macrophages with oxLDL as an inflammation inducer. After oxLDL treatment, the mRNA expression of tumor necrosis factor α (*Tnfα*), inducible nitric oxide synthase (*iNos*), interleukin-6 (*Il6*), and interleukin-1β (*Il1β*) was downregulated in RNF128-deficiency macrophages (Fig. S5c).

To further evaluate the effect of RNF128 on SRB1, human embryonic kidney 293T (HEK293T) cells were transfected with Myc-tagged SRB1 (Myc-SRB1) plasmid accompanied by Flag-RNF128 or Flag-Vector. SRB1 protein level was upregulated by RNF128, whereas the expression of other molecules, including CD36, SRA1, ABCA1, and ABCG1, was equivalent between these two groups (Fig. S6a, b). Additionally, the RNF128 plasmid was transfected into HEK293T cells according to concentration gradients positively correlated with SRB1 protein level (Fig. 3F and S6c). A similar trend was observed in macrophages incubated with a growing multiplicity of infection (MOI) of adenovirus carrying RNF128 (Fig. S6d), validating the stabilization of SRB1 by RNF128. SRB1 was originally identified as a scavenger receptor for modified LDL binding; thus, we believe that RNF128 deficiency downregulated SRB1 protein and diminished modified lipoprotein uptake and foam cell formation.

RNF128 stabilizes SRB1 through intervention in lysosomal degradation

RNF128 knockout in macrophages reduced the SRB1 protein level without altering its mRNA level, suggesting the existence of post-transcriptional regulation of RNF128. Therefore, we sought to

https://doi.org/10.1038/s41467-025-57404-6

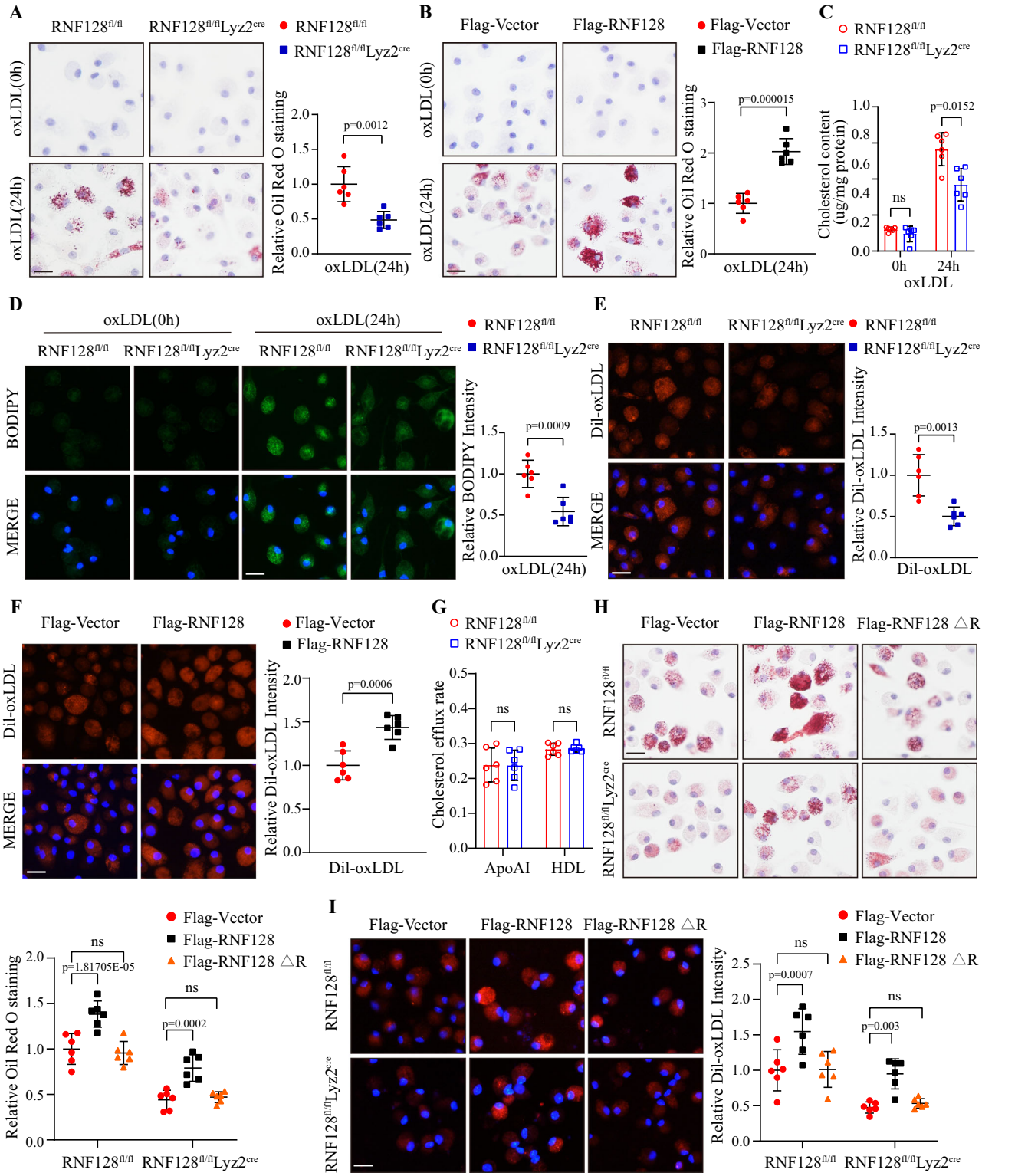

investigate whether RNF128 regulated SRB1 by monitoring SRB1 protein stability. After preincubation with oxLDL for 12 h, RNF128-deficient, and control macrophages were treated with cycloheximide (CHX, 5 μg/mL) at different durations to inhibit cellular protein synthesis. Protein expression was quantified through Western blotting, which demonstrated that RNF128 deficiency accelerated the degradation of SRB1 protein (Fig. S6e), and a similar trend was observed in macrophages from RNF128-CKO and WT mice (Fig. 3G).

As the proteasome system and lysosome pathway are two major mechanisms for intracellular protein degradation, we next investigated the blocking of specific degradation pathways by RNF128, initiating protein stability of SRB1. Chloroquine (CQ, 5 μmol/L), bafilomycin A1 (BAF-A1, 10 μmol/L), and ammonium chloride (NH_4Cl,10 μmol/L) inhibit endosomal acidification, thereby preventing autophagosome fusion with the lysosome. 3-methyladenine (3-MA, 5 μmol/L) inhibits autophagy by blocking autophagosome formation, while SAR405 (10 μmol/L), can inhibit vesicle trafficking from late endosomes to lysosomes. RNF128-deficient macrophages were treated with dimethyl sulfoxide (DMSO) and proteasome and lysosome inhibitors. Compared to that in control macrophages, SRB1 protein was

Fig. 2 | Macrophage-specific deletion of RNF128 attenuates foam cell formation via reducing lipid uptake. A Oil Red O staining of macrophages derived from $RNF128^{fl/fl}Lyz2^{cre}$ mice (macrophage-specific conditional RNF128 knockout) and $RNF128^{fl/fl}$ mice (the control group) incubated with oxLDL (75 μg/mL) (left). Quantitative analysis was shown (right, $n = 6$). Scale bar: 20 μm. **B** Oil Red O staining of macrophages overexpressed with Flag-RNF128 or a control vector incubated with oxLDL (left). Quantitative analysis was shown (right, $n = 6$). Scale bar: 20 μm. **C** Total cholesterol content of macrophages from $RNF128^{fl/fl}Lyz2^{cre}$ mice and $RNF128^{fl/fl}$ mice incubated with oxLDL ($n = 6$). **D** Neutral lipid dyed with boron-dipyrrolemethene (BODIPY) of macrophages isolated from $RNF128^{fl/fl}Lyz2^{cre}$ mice and $RNF128^{fl/fl}$ mice with oxLDL (left). Quantitative analysis was shown (right, $n = 6$). Scale bar: 20 μm. **E** Macrophages derived from $RNF128^{fl/fl}Lyz2^{cre}$ mice and $RNF128^{fl/fl}$ mice were treated with oxLDL labeled by red fluorescent probe (Dil-oxLDL) (20 μg/mL) for 6 h. Representative images of Dil-oxLDL uptake and quantitative intensity analysis was shown ($n = 6$). Scale bar: 20 μm. **F** Representative images of Dil-oxLDL uptake and quantitative intensity analysis in macrophages overexpressed with Flag-RNF128 or a control vector ($n = 6$). Scale bar: 20 μm. **G** Cholesterol efflux assay of macrophages derived from $RNF128^{fl/fl}Lyz2^{cre}$ mice and $RNF128^{fl/fl}$ mice with Apolipoprotein A-I (ApoAI) and high-density lipoprotein (HDL) incubation, respectively ($n = 6$). **H**, **I** Macrophages derived from $RNF128^{fl/fl}Lyz2^{cre}$ mice and $RNF128^{fl/fl}$ mice were overexpressed with Flag-RNF128, Flag-RNF128 ΔR or a control vector. Images of Oil Red O staining (**H** with oxLDL stimulation for 24 h) and uptake assay (**I** with Dil-oxLDL treatment for 6 h). Quantitative analysis was shown ($n = 6$). Scale bar: 20 μm. The "*n*" represents the number of biologically independent samples. Data were presented as mean ± SD, normal distribution was tested by Shapiro–Wilk method. Two-way ANOVA followed by Tukey post hoc test was used for (**H**). Mann–Whitney test (two-tailed) was used for (**C**, **G**). Kruskal–Wallis test followed by a Dunn test was used for (**I**). Unpaired two-tailed Student's *t*-test was used for the others. ns not significant. Source data are provided as a Source Data file.

decreased in RNF128-deficient macrophages, both of which were incubated with DMSO only. Inhibition of lysosomal function by CQ, BAF-A1, and NH_4Cl markedly abrogated this decrease. However, MG-132 (10 μmol/L), an inhibitor of proteasome activity, did not affect SRB1 expression (Fig. S6g [left] and S6h [left]). Treatment with other lysosome pathway inhibitors, 3-MA and SAR405, resulted in upregulation of SRB1 protein. In contrast, proteasome inhibitors, including bortezomib (100 nmol/L) and N2, N4-dibenzylquinazoline-2,4-diamine (DBeQ, 10 μmol/L), had no effect on SRB1 protein levels in macrophages (Fig. S6g [right] and S6h [right]). Similar results were obtained using macrophages derived from RNF128-CKO mice (Fig. 3H and S6f). These results indicate that RNF128 upregulated the SRB1 protein level by suppressing its lysosomal protein degradation.

Then, we explored whether RNF128 stabilized SRB1 through E3 ligase activity. The co-expression of SRB1 with RNF128 in HEK293T cells enhanced the SRB1 protein level, whereas RNF128 ΔR lost the function for stabilization (Fig. 3I and S6i). A similar trend was detected in macrophages with RNF128 or RNF128 ΔR overexpression (Fig. S6j). Finally, a recovery experiment was performed to confirm that SRB1 protein can be restored with an approximately twofold increase after RNF128 overexpression in macrophages from RNF128-CKO mice. However, the rescue effect was negated by RNF128 ΔR (Fig. 3J and S6k).

SRB1 involves in the effects of RNF128 on foam cell formation

Furthermore, we performed the rescue experiments that SRB1 protein was recovered through adenovirus-mediated overexpression (Flag-SRB1) in $RNF128^{fl/fl}Lyz2^{cre}$ macrophages. The Dil-oxLDL uptake ability was strengthened compared to that in the control group (Flag-Vector). For macrophages from $RNF128^{fl/fl}$ mice, overexpressed SRB1 also slightly enhanced Dil-oxLDL influx (Fig. 3K, M [left]). Consequently, lipid accumulation was rescued through SRB1 overexpression (Fig. 3L, M [right]). To further verify the role of SRB1 with RNF128 on foam cell formation, we constructed an SRB1-gene knockout RAW264.7 cell line using the CRISPR/Cas9 system. RAW264.7 cells without SRB1 knockout was defined as the control group (SRB1-Ctrl) while cells with SRB1 stable knockout was the SRB1-KO group. We overexpressed RNF128 and discovered that without SRB1, RNF128-overexpression could not promote lipid uptake and accumulation obviously (Fig. S6l–m).

These findings were confirmed using HeLa cells transfected with SRB1 and control plasmids incubated with Dil-oxLDL. Cells transfected with SRB1 had an approximately fourfold increase in fluorescence intensity of Dil-oxLDL compared with control cells (Fig. S7a). In addition, SRB1-knockdown macrophages were obtained via siRNA (SRB1-Si), featuring an impaired internalization ability of Dil-oxLDL compared to that in the negative control cells (SRB1-NC) (Fig. S7b). Moreover, laser confocal microscopy revealed the colocalization between SRB1 and Dil-oxLDL in macrophages (Fig. S7c), which is more pronounced in HeLa cells in which SRB1 was overexpressed (Fig. S7d). Besides in vitro experiments, we also confirmed the function of SRB1 for lipid uptake in vivo. Adeno-associated virus encoding a macrophage-specific short hairpin RNA (shRNA) were intravenously administered to male mice aged 6 weeks, followed by a WD feeding for 15 weeks. Mice of the control group (Ctrl) were treated with AAV-Lyz2-shRNA-control, while mice of the SRB1 Lyz2-shRNA group were injected with AAV-Lyz2-shRNA-SRB1 for the downregulation of SRB1 in macrophages. Primary macrophages were isolated from mice of the control group and SRB1 Lyz2-shRNA group to confirm the knockdown efficiency of SRB1 (Fig. S7e). To evaluate oxLDL uptake in vivo, following receipt of WD, mice were injected retro-orbitally with Dil-oxLDL for 1 h. Similarly sized plaques were isolated from the thoracic aorta for confocal fluorescence microscopy detection. Three-dimensional depiction of Dil-oxLDL localization and representative cumulative images demonstrated that far less Dil-oxLDL entered the plaque of the SRB1 Lyz2-shRNA group compared to controls (Fig. S7f, g). Overall, these data highlight the role of SRB1 as a target for RNF128 to facilitate oxLDL uptake and lipid droplet accumulation.

RNF128 interacts with the extracellular region of SRB1 protein through the PA domain

We co-transfected HEK293T cells with a green fluorescent protein (GFP)-tagged RNF128 plasmid and other plasmids encoding molecules relating to lipid uptake and efflux for the co-immunoprecipitation (Co-IP) experiment. RNF128 interacted with SRB1 protein compared to others, such as SRA1, CD36, CD68, ABCA1, and ABCG1 (Fig. 4A and S8a). Then, we confirmed the interaction between RNF128 and SRB1 using tag-altered plasmids (Fig. 4B and S8b). Endogenous Co-IP in macrophages with RNF128 or SRB1 antibodies verified this efficient interaction. Besides, the level of immunoprecipitated protein declined in a time-dependent manner in response to various durations of oxLDL treatment (Fig. 4C and S8c). Purified recombinant proteins were also used to validate the direct binding in vitro (Fig. 4D). Moreover, confocal microscopy revealed that RNF128 was sufficiently colocalized with SRB1 in HeLa cells (Fig. 4E).

To investigate the binding domains required for the RNF128–SRB1 interaction, we truncated RNF128 into the following fragments: full-length RNF128 without RING domain (RNF128-ΔR), full-length RNF128 lacking signal peptide (RNF128-ΔSP), N-terminus containing the signal peptide and protease-associated (PA) domain (RNF128-N), RNF128-N along with transmembrane domain (RNF128-ΔC), C-terminus containing the RING finger (RNF128-C), and RNF128-C added with transmembrane domain (RNF128-ΔN) (Fig. 4F). All Flag-tagged fragments were transfected into HEK293T cells with Myc-SRB1. The Co-IP analysis demonstrated that besides full-length RNF128 (RNF128-WT), RNF128-ΔR, RNF128-N, and RNF128-ΔC interacted with SRB1. In contrast, the remaining three fragments lost the ability (Fig. 4G), indicating that the N-terminus was required for this binding.

The signal peptide at the N-terminus is an essential component for the correct targeting and transport pathway of many proteins[37,38].

https://doi.org/10.1038/s41467-025-57404-6

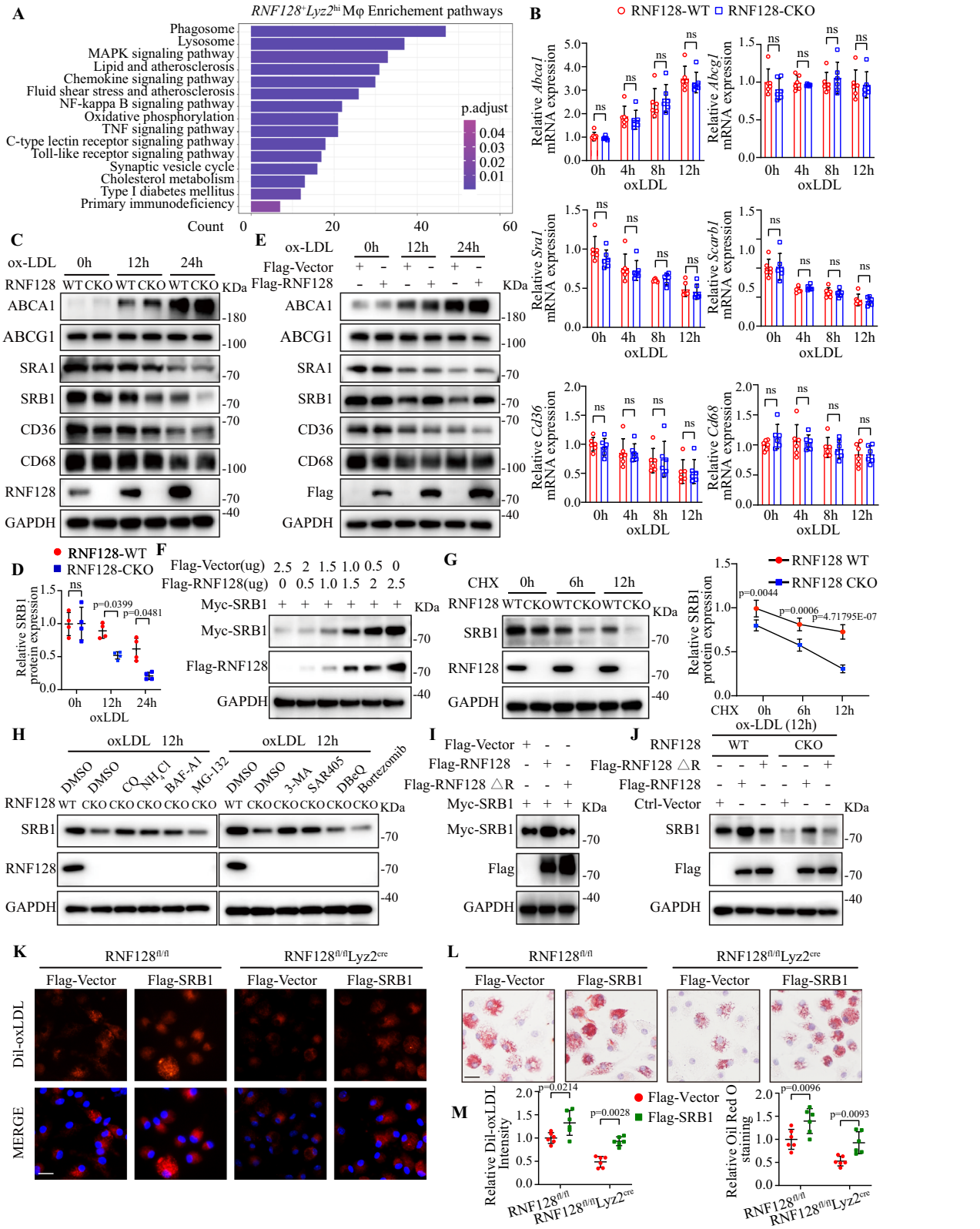

Therefore, we hypothesized that RNF128-ΔSP could not be conveyed to the SRB1-riched area for interaction due to transport incompetence. Then, we aimed to identify the specific domain in the N-terminus that bound with SRB1. The PA domain of RNF128 is evolutionarily conserved (Fig. S8d) and captures target proteins for cytosolic ubiquitination[29,39]. Therefore, we constructed an RNF128 deletion mutant of the PA domain (RNF128-ΔPA) and a GFP-tagged recombinant plasmid containing the sequence for the PA domain only (RNF128-PA). RNF128 lost the ability to interact with SRB1 protein owing to the absence of the PA domain, whereas RNF128-PA was efficiently bound with SRB1 (Fig. 4H).

Then, we generated three truncated forms of SRB1 constructs: SRB1-ΔN (amino acids [aa] 11–509), SRB1-ΔEXT (aa 1–33,340–509), and SRB1-ΔC (aa 1–462) (Fig. 4I). Co-IP experiment revealed that SRB1

Fig. 3 | RNF128 deficiency downregulates SRB1 protein level and inhibits foam cell formation. A Kyoto Encyclopedia of Genes and Genomes (KEGG) pathway enrichment focusing on *RNF128*^{n}*Lyz2*^{hi} macrophages. **B** Quantitative PCR analysis of indicated gene expression in macrophages from RNF128-CKO and RNF128-WT mice after oxLDL stimulation. Target gene expression was normalized to *Actin* mRNA level ($n = 6$). **C** Western blotting images of indicated proteins from different groups. GAPDH was used for normalization ($n = 4$). **D** Quantitative analysis of SRB1 protein level in Fig. 3C ($n = 4$). **E** Western blotting analysis of indicated proteins with or without RNF128 overexpression ($n = 4$). **F** Western blotting images of indicated proteins in HEK293T cells transfected with a concentration gradient of Flag-RNF128. Cells in each sample were transfected with the same amount of plasmids coding for Myc-SRB1. Similar results were repeated independently for four times. **G** Western blotting images of indicated proteins and the statistical quantification ($n = 4$). **H** Western blotting images of indicated proteins in macrophages from RNF128-CKO and WT mice, which were treated with different inhibitors for 6 h after oxLDL treatment for 12 h ($n = 4$). **I** Western blotting images of indicated proteins in HEK293T cells transfected with plasmids encoding Myc-SRB1 along with the control vector, wild-type Flag-RNF128 or Flag-RNF128 ΔR ($n = 4$). **J** Western blotting images of indicated proteins in macrophages from different groups ($n = 4$). **K** Representative images of macrophages from RNF128$^{fl/fl}$Lyz2^{cre} mice and RNF128$^{fl/fl}$ mice with or without Flag-SRB1 overexpression. Scale bar: 20 μm. **L** Oil Red O staining of macrophages from indicated groups incubated with oxLDL for 24 h ($n = 6$). Scale bar: 20 μm. **M** Data analysis of (K, left) and (L, right). The "*n*" represents the number of biologically independent samples. Data were presented as mean ± SD, normal distribution was tested by Shapiro–Wilk method. Adjusted *P* values for (**A**) were determined using a two-tailed test. Two-way ANOVA followed by Tukey post hoc test was used for (**B**, **G**, **M**, right). Mann–Whitney test (two-tailed) was used for (**D**, **M**, left). Adjustments were made for multiple comparisons. Source data are provided as a Source Data file.

lacking extracellular domain (SRB1-ΔEXT) could not interact with RNF128 (Fig. 4J), indicating that RNF128 interacts with the extracellular region of SRB1 protein via its PA domain.

RNF128 catalyzes K63-linked polyubiquitin chains of SRB1 at lysine 478

Because lysosomal degradation of protein is usually associated with ubiquitylation[23,40], we investigated whether RNF128 regulated SRB1 protein by ubiquitylation. First, HEK293T cells were transfected with Myc-tagged SRB1, Flag-tagged RNF128, and hemagglutinin (HA)-tagged ubiquitin, including wild-type ubiquitin (Ub) and mutant ubiquitin (K48 and K63), whose lysine (K) residues were substituted with arginine (R) except the lysine at positions 48 or 63, respectively. Western blotting analysis revealed that polyubiquitination of SRB1 was catalyzed by RNF128 in the presence of Ub or K63 rather than K48 (Fig. 5A). However, this effect was sharply declined in both RNF128 ΔR and point mutant RNF128 C2A (C277A and C280A, with cysteine residues at positions 277 and 280 replaced by alanine) transfected cells (Fig. 5B and S9a), suggesting that the E3 ligase activity was required for the polyubiquitination of SRB1. Cysteines at positions 277 and 280 within the RING region were highly conserved among different species (Fig. S9b). They might be necessary for E3 catalytic activity, which was consistent with the reported results[41].

Next, we tested the RNF128-mediated ubiquitination of endogenous SRB1 in macrophages and observed that SRB1 was ubiquitinated in both K48-linked and K63-linked chains. However, the levels of wild-type Ub- and K63-linked polyubiquitination were much lower in RNF128-deficient macrophages than in control cells with oxLDL treatment. In contrast, the amount of K48-linked ubiquitination of SRB1 did not respond to RNF128 deletion (Fig. S9c), which was verified in macrophages isolated from RNF128-CKO mice (Fig. 5C) and RNF128-overexpressed macrophages (Fig. S9d). Therefore, these observations indicated that RNF128 targeted K63 polyubiquitination of SRB1. Finally, we explored the catalyzation of polyubiquitination by RNF128 in the presence of wild-type ubiquitin and ubiquitin K63 rather than ubiquitin K48 through in vitro ubiquitination assay (Fig. 5D).

The catalytic domain of RNF128 is intracellular, and the cytosolic C-terminus of SRB1 is critical for uptake and transcytosis of lipoproteins[17]. Therefore, we assumed that lysine residues responsible for RNF128-mediated polyubiquitination of SRB1 might be intracellular. Based on the SRB1 protein structure, we transfected Myc-SRB1 (including SRB1-ΔN and SRB1-ΔC), ubiquitin K63, and Flag-tagged RNF128 into HEK293T cells. RNF128 promoted K63-linked ubiquitination of both SRB1 and SRB1-ΔN, excluding SRB1-ΔC, suggesting that the C-terminus exhibited a central role in K63-linked ubiquitination by RNF128 (Fig. 5E).

SRB1 possesses nine lysine or cysteine residues intracellularly. To identify the accurate modification site, we constructed variants with point mutations SRB1 K6R, SRB1 K469R, SRB1 K478R, SRB1 K479R, SRB1 K482R, SRB1 K484R, SRB1 K500R, and SRB1 K508R by replacing the lysine residues at positions 6, 469, 478, 479, 482, 484, 500, and 508 with arginine, respectively, and constructed SRB1 C3A by substituting the cysteine residue at position 3 with alanine (Fig. S9e). Co-transfection and Co-IP analysis of HEK293T cells revealed that the K63-linked ubiquitination promotion was almost extinct in cells transfected with SRB1 K478R in the presence of RNF128 (Fig. 5F, G). Moreover, we generated the mutant SRB1-K0 (C- and N-termini) by replacing all lysine and cysteine residues in N- and C-termini of SRB1 with arginine and alanine, respectively. Then, the single-lysine mutants were generated by reintroducing individual lysine residues into SRB1-K0 (C- and N-termini) (Fig. S9f). RNF128 modulated the K63-linked polyubiquitination of SRB1 K478, which was highly conserved in humans and mice (Fig. 5H). Recovery experiments revealed that overexpression of RNF128 rescued the amount of Ub- and K63-linked ubiquitination (Fig. 5I). However, the RNF128 ΔR mutant had no function in rescue, and K48-linked ubiquitination was free from the effect of RNF128 (Fig. 5I). Collectively, these data demonstrate that RNF128 catalyzes the K63-linked polyubiquitination of RNF128 at lysine 478.

RNF128-mediated ubiquitination of SRB1 promotes its recycling to the membrane via Rab11

The localization to the plasma membrane is deduced from the biotinylation of intact cells and avidin affinity purification from whole cell lysates. After the treatment with oxLDL for indicated time points, macrophages were incubated with biotin. This biotinylation process was prepared for plasma membrane protein extraction. Plasma membrane SRB1 proteins determined by labeling with biotin were extracted and quantified through Western blotting. RNF128-deficient macrophages exhibited lower membrane SRB1 levels than control cells after oxLDL stimulation (Fig. S10a). Consistent results were obtained in macrophages with the genetic absence of RNF128 (Fig. 6A and S10b) and overexpressed RNF128 (Fig. S10c). Besides, a greater colocalization of SRB1 and LAMP2 (lysosomal-associated membrane protein 2) was observed in control cells than in RNF128-overexpressed HeLa cells. To quantify the LAMP2-associated SRB1 protein level, the Co-IP assay in macrophages was performed, which revealed that after RNF128 overexpression, the interaction between SRB1 and LAMP2 was reduced. Therefore, Membrane SRB1 protein in cells transfected with RNF128 was more easily detectable (Fig. 6B, C and S10d). These findings indicated that RNF128 preserved membrane SRB1 protein by preventing it from degradation by the lysosome. We transfected RNF128 or control vector in HEK293T cells expressing SRB1 or SRB1 mutant, SRB1 K478R. Compared with the control group, RNF128 overexpression increased the protein level of SRB1 in the membrane. In contrast, the expression of SRB1 K478R was unaffected by RNF128 at both total and membranal levels (Fig. 6D and S10e).

https://doi.org/10.1038/s41467-025-57404-6

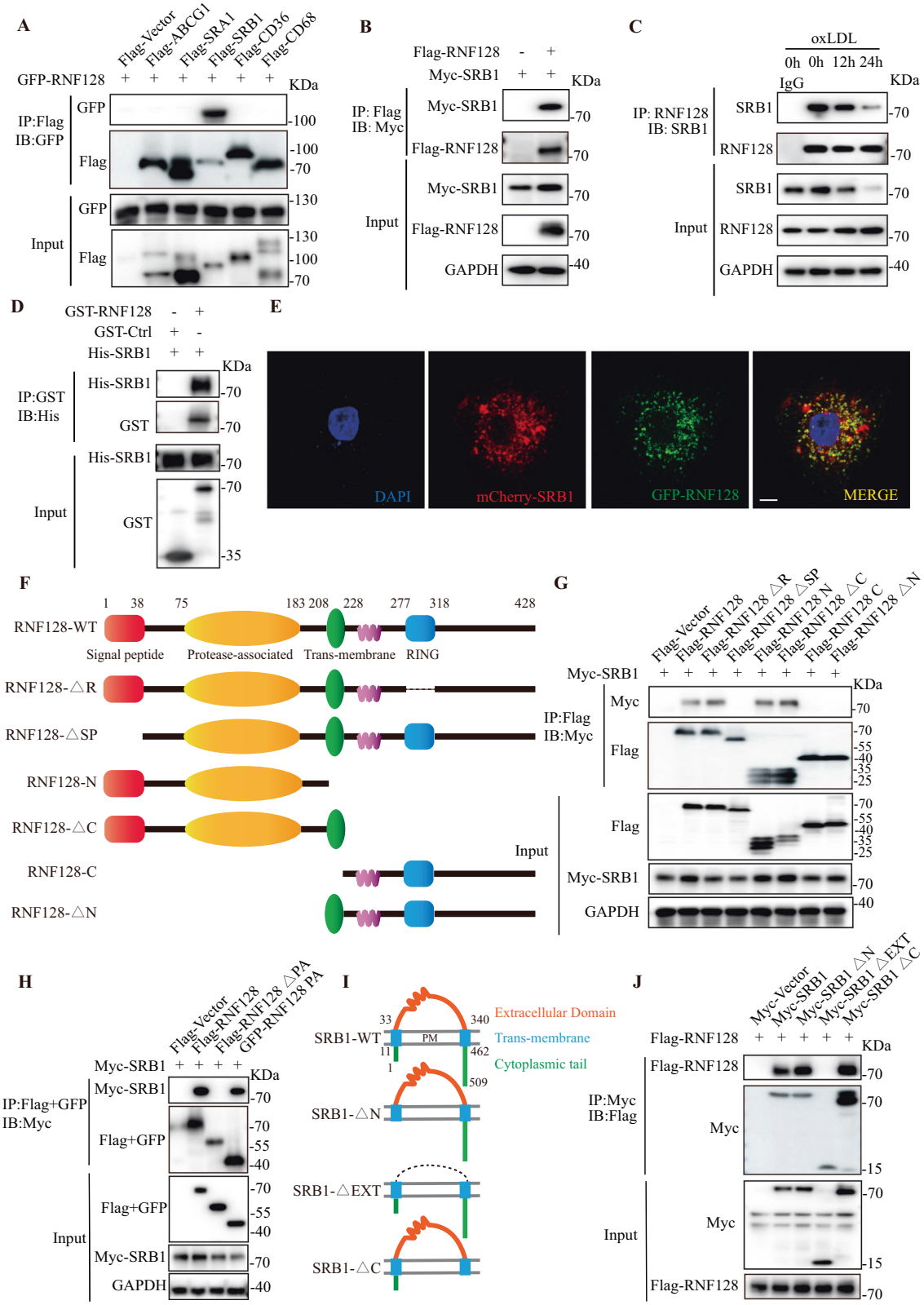

As more SRB1 proteins were retained in the membrane, the mechanism of SRB1 membranal and intracellular trafficking required investigation. Rab protein (small GTP-binding protein) is a regulator for lipid transport[42], where Rab4 directs recycling from early endosomes to the plasma membrane, and Rab11 modulates the transport of perinuclear vesicles back to the cell surface[43,44]. scRNA-seq data revealed that phagosome and lysosome pathways were enriched (Fig. 3A). Therefore, we transfected Rab4, Rab11, or control siRNA into HEK293T cells already overexpressed with SRB1, RNF128, or the control vector, to determine whether SRB1 trafficking was regulated by the endocytic recycling pathway. RNF128 contributed to SRB1 retention in the membrane, whereas this contribution was markedly abolished

Fig. 4 | RNF128 interacts with the extracellular region of SRB1 protein via the PA domain. A Co-immunoprecipitation (Co-IP) analysis of HEK293T cells co-transfected with a green fluorescent protein (GFP)-tagged RNF128 and Flag-tagged ABCG1, SRA1, SRB1, CD36, CD68 to examine the interactors of RNF128. Co-IP of whole cell lysates was immunoprecipitated using Flag beads. **B** Co-IP assay of HEK293T cells co-transfected with Myc-SRB1 and Flag-RNF128. Co-IP was performed using Flag beads. **C** Western blotting images of indicated proteins of endogenous Co-IP in macrophages immunoprecipitated with anti-RNF128 or rabbit IgG antibody under oxLDL (75 μg/mL) stimulation for different time points. **D** In vitro Co-IP analysis of RNF128-SRB1 interaction using purified recombinant proteins including Glutathione S-transferase (GST)-tagged RNF128 and His-tagged SRB1. **E** Representative confocal microscopic images of colocalization between RNF128 and SRB1 in HeLa cells co-transfected with GFP-tagged RNF128 and mCherry-tagged SRB1. Scale bar: 10 μm. **F** Schematic diagram of wild-type Flag-RNF128 and its truncated mutants. **G**, **H** Co-IP analysis of the interaction between Myc-SRB1 with Flag-RNF128 and its truncated forms in HEK293T cells. **I** Schematic diagram of Myc-SRB1 and its truncated mutants. **J** Co-IP analysis of the interaction between Flag-RNF128 with Myc-SRB1 and its truncated forms in HEK293T cells. Each experiment was repeated independently with similar results four times. Source data are provided as a Source Data file.

when Rab11 was silenced. In contrast, Rab4 deficiency did not affect the expression of membrane SRB1. To avoid the off-target siRNA effects, we transfected the His-tagged control vector and Rab11 plasmids, respectively, based on the treatment of Rab11 deficiency mediated by siRNA and results showed that Rab11 overexpression upregulated SRB1 protein level on the membrane, indicating the central role of Rab11 in SRB1 recycling (Fig. 6E and S10f).

SRB1 was colocalized with several endosome markers[45]. From Co-IP analysis, we discovered that after RNF128 knockout, the interaction between SRB1 and Rab11 was reduced in macrophages with oxLDL treatment (Fig. 6F and S10g). Similarly, overexpressed RNF128 promoted their interaction (Fig. 6G and S10h). Laser confocal microscopy confirmed a higher colocalization between SRB1 and Rab11 in HeLa cells after RNF128 was transfected (Fig. 6H). RNF128 modulated both membrane and total SRB1 protein; as increased SRB1 expression on the cell surface is reflected in increased total SRB1 protein level, hence, determining whether increased SRB1 proteins in the membrane were independent of the increased total SRB1 proteins was necessary. From our results above, RNF128 stabilizes SRB1 through intervention in lysosomal degradation. Therefore, we intended to prevent SRB1 from lysosomal degradation so that the total SRB1 protein level could be constant. If membrane SRB1 protein level still could be regulated independently of total SRB1 level, recycling might be the primary event leading to decreased degradation. As our previous experiments showed that RNF128 influences SRB1 only under oxLDL stimulation, oxLDL incubation was applied to cells in all experimental groups. CQ, 3-MA, and leupeptin were lysosomal degradation inhibitors and used to inhibit SRB1 from lysosomal degradation respectively, and the Co-IP assay revealed that in each group using inhibitors, less SRB1 was combined with Rab11 in RNF128-genetically silent macrophages than that in control cells (Fig. 6I, J [upper]); however, total SRB1 proteins had already been prevented from degradation (Fig. 6I, J [bottom]). We then extracted membrane proteins as described (Fig. S10i), and consequently, membrane SRB1 proteins presented a consistent trend (Fig. 6K and S10j). After RNF128 knockout, the transport of SRB1 from the cytoplasm to the cell membrane is reduced, resulting in a decrease in SRB1 detected on the membrane. Additionally, more SRB1 in the cytoplasm undergoes degradation, leading to a reduction in total SRB1. After inhibitor treatment, the recovery of total SRB1 protein levels in the RNF128-KO group is related to the inhibition of lysosomal degradation, while SRB1 on the cell membrane remained relatively stable. This indicates that the function of RNF128 KO in suppressing SRB1 recycling to the cell membrane persists and is not influenced by downstream lysosomal pathways. These results demonstrated that RNF128 assisted the recycling of more SRB1 proteins to the plasma membrane when combined with Rab11. Thus, RNF128 and Rab11-dependent recycling leads to decreased degradation and increased levels of SRB1.

Finally, we determined whether this pro-recycling function relied on the E3 ligase activity of RNF128 and K63-linked ubiquitination of SRB1 and observed that RNF128 lost the ability to facilitate the combination of SRB1 and Rab11 in the absence of the RING domain (RNF128 ΔR) (Fig. 6L and S10k). In addition, RNF128 could not promote the interaction between Rab11 and SRB1 mutant, SRB1 K478R (Fig. 6M and S10 l).

Macrophage-specific deletion of RNF128 ameliorates atherosclerosis in male and female mice

$RNF128^{fl/fl}Lyz2^{cre}$ mice and $RNF128^{fl/fl}$ mice were crossed with $ApoE^{-/-}$ mice to generate $ApoE^{-/-}RNF128^{fl/fl}Lyz2^{cre}$ and $ApoE^{-/-}RNF128^{fl/fl}$ mice as the experimental and control groups, respectively, to evaluate the role of macrophage-RNF128 in the development of atherosclerosis in vivo. Both male and female mice of the two groups were fed WD at six weeks of age, and after 20 weeks of WD, mice were euthanized, and a detailed analysis of atherosclerosis was conducted (Fig. S11a). $ApoE^{-/-}RNF128^{fl/f}$ mice exhibited more severe atherosclerosis than $ApoE^{-/-}RNF128^{fl/fl}Lyz2^{cre}$ mice in both males and females from the representative in situ images (Fig. 7A and S12a). The deletion of macrophage-RNF128 reduced the atherosclerotic lesion area in the en face aortas stained with Oil Red O (Fig. 7B and S12b). Additionally, atherosclerotic lesion area from aortic root sections of $ApoE^{-/-}RNF128^{fl/fl}Lyz2^{cre}$ mice was decreased by ~23 and 32% compared with that of $ApoE^{-/-}RNF128^{fl/fl}$ mice in males and females, respectively (Fig. 7C and S12c). Similar trends were observed in the aortic roots stained with Oil Red O (Fig. 7D and S12d). Moreover, immunofluorescent staining in cross-sectional lesions revealed that loss of RNF128 in macrophages reduced SRB1 expression in the atheroma (Fig. 7E and S12e), confirming that RNF128 deficiency in macrophages downregulated SRB1 protein level and alleviated atherosclerosis. Inflammatory cytokines, including TNFα, IL1β, and IL6 within plaques, were examined using immunohistochemistry (IHC), which revealed a significant reduction of inflammation in $ApoE^{-/-}RNF128^{fl/fl}Lyz2^{cre}$ mice compared with $ApoE^{-/-}RNF128^{fl/fl}$ mice (Figs. S11b, S12f). Besides, compared with $ApoE^{-/-}RNF128^{fl/fl}$ mice, the Masson's Trichrome analysis showed an increase in collagen content in $ApoE^{-/-}RNF128^{fl/fl}Lyz2^{cre}$ mice (Fig. S11c). Therefore, RNF128 inhibition might not only slow atherogenesis, but also lead to a stabilization of the plaque phenotype. In addition, body weight and plasma levels of triglyceride (TG), total cholesterol (CHO), low-density lipoprotein cholesterol (LDL-C), and high-density lipoprotein cholesterol (HDL-C) were comparable between the two groups (Figs. S11d, S12g).

To verify the athero-protective role of RNF128 deficiency, an LDLR-deficiency model was generated through AAV-PCSK9 (proprotein convertase subtilisin/kexin type 9) intravenous injection of both $RNF128^{fl/fl}Lyz2^{cre}$ and $RNF128^{fl/fl}$ mice at the age of 6 weeks, followed by WD feeding for 20 weeks (Fig. S13a). A similar trend was observed in both males and females (Fig. S13b–h). Overall, our results reveal that RNF128 in macrophages exhibits a pro-atherosclerotic role by facilitating lipid deposition and reducing inflammation.

To establish the functional connection between RNF128 and SRB1 in an atherosclerosis model, an AAV harboring a macrophage-specific promoter was constructed and intravenously injected into male mice aged 6 weeks following a WD feeding for 20 weeks. $ApoE^{-/-}RNF128^{fl/fl}$ mice were administered with AAV-Lyz2 control vector ($ApoE^{-/-}RNF128^{fl/fl}$) and $ApoE^{-/-}RNF128^{fl/fl}Lyz2^{cre}$ were administered with AAV-Lyz2 control vector ($ApoE^{-/-}RNF128^{fl/fl}Lyz2^{cre}$) and AAV-Lyz2 SRB1 ($ApoE^{-/-}RNF128^{fl/fl}Lyz2^{cre}$ + SRB1 Lyz2-AAV), respectively. Primary macrophages were isolated from mice to confirm the overexpression of SRB1 (Fig. S11e). AAV-Lyz2 SRB1 administration had no marked effects on body weight gain or serum lipid levels (Fig. S11f). RNF128 deficiency in macrophages ameliorates atherosclerosis, while macrophage SRB1 administration

https://doi.org/10.1038/s41467-025-57404-6

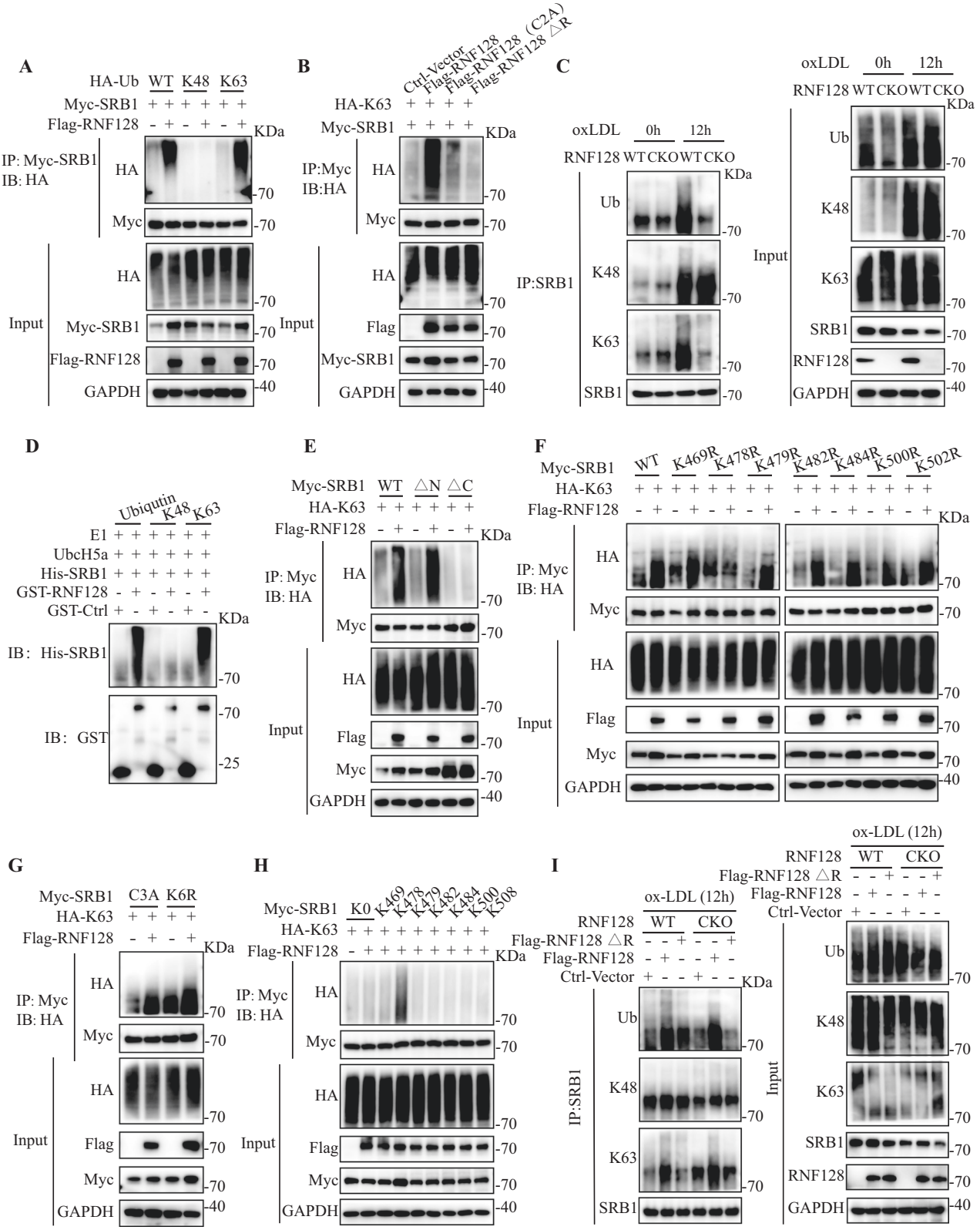

promoted plaque formation in the aortas and aortic roots in ApoE$^{-/-}$ RNF128$^{fl/fl}$Lyz2^{cre} mice (Fig. 7F–J), which was consistent with our in vitro findings that SRB1 was required for the pro-atherosclerotic effect of RNF128.

Discussion

Most recent studies have substantiated the effect of SRB1 on HDL metabolism and reverse cholesterol transport (RCT) in hepatocytes, and the growing importance of SRB1 in modified LDL has also become apparent. SRB1 exhibits a highly similar protein structure and the same ligand-binding interface with CD36 and LIMP2 analyzed by homology modeling, suggesting that SRB1 may function as a lipid-uptake receptor-like CD36 to facilitate macrophage foam cell formation[14,15,46,47]. It is intriguing to note that human SRB1 is expressed highly in macrophages of atherosclerotic lesions[48]. SRB1 is present in low levels in monocytes, and its expression amplifies with differentiation to

Fig. 5 | RNF128 catalyzes K63-linked polyubiquitin chains of SRB1 at lysine 478. **A** Co-IP analysis of SRB1 ubiquitination in HEK293T cells transfected with Myc-tagged SRB1 (Myc-SRB1), Flag-tagged RNF128 (Flag-RNF128) and hemagglutinin (HA)-tagged ubiquitin (Ub) and mutant ubiquitin (K48 and K63). **B** Co-IP analysis of SRB1 ubiquitination in HEK293T cells transfected with plasmids encoding Myc-SRB1 and HA-K63, as well as a control vector or plasmids encoding Flag-RNF128, Flag-RNF128 ΔR or point mutant RNF128 C2A. **C** Co-IP analysis of endogenous SRB1 ubiquitination in macrophages from RNF128-CKO and RNF128-WT mice with or without oxLDL (75 μg/mL) stimulation for 12 h. **D** In vitro SRB1-ubiquitination assay with purified recombinant proteins including glutathione *S*-transferase (GST)-tagged RNF128 and His-tagged SRB1 in the presence of E1, E2 (UbcH5a), ubiquitin (wildtype), ubiquitin (K63), or ubiquitin (K48). **E** Co-IP analysis of SRB1 ubiquitination in HEK293T cells transfected with HA-K63, Flag-RNF128 or a control vector in the presence of Myc-SRB1 and its mutants including SRB1-ΔN and SRB1-ΔC. **F**, **G** Co-IP analysis of the polyubiquitination of Myc-SRB1, its C- (**F**) and N-terminal (**G**) mutants in HEK293T cells co-transfected with HA-K63, Flag-RNF128 or a control vector. **H** Co-IP analysis of the polyubiquitination of Myc-SRB1 and its mutants in HEK293T cells co-transfected with plasmids encoding HA-K63, Flag-RNF128, or a control vector. **I** Co-IP analysis of endogenous SRB1 ubiquitination in macrophages from RNF128-CKO and RNF128-WT mice with Flag-RNF128 or Flag-RNF128 ΔR overexpression with oxLDL treatment. Each experiment was repeated independently with similar results four times. Source data are provided as a Source Data file.

macrophages[49], suggesting a considerable role of SRB1 in macrophages during atherosclerosis development. SRB1 was originally identified as a scavenger receptor attributed to its combination with modified LDL[50], and the binding affinity of SRB1 is greater with oxLDL than with other lipoproteins. Based on the fact that oxidation is more likely to instigate lipid accumulation than other lipoprotein modifications[22], we regarded SRB1 as a pro-atherogenic factor. The pro-atherogenic role of SRB1 was first established due to its function in promoting LDL and oxLDL transcytosis in endothelial cells, contrary to its role in hepatocytes[18]. However, in macrophages, the role of SRB1 remains controversial. SRB1-mediated oxLDL internalization was detected in our study, demonstrating that RNF128 stabilized the SRB1 protein level and facilitated foam cell formation. Furthermore, with the recovery experiment where SRB1 expression was rescued in RNF128-deficient macrophages, lipid deposition aggravated subsequently, indicating that macrophage SRB1 was involved in the process that RNF128 augmented lipid uptake and accumulation.

Similar to the phagocytosis of oxLDL through clathrin-mediated endocytosis by SRA1, oxLDL can be internalized and degraded through the endocytic pathway mediated by SRB1[16,22]. During lipid-mediated endocytosis, oxLDL is bound to the receptors and delivered to endosomes. Then receptors dissociated from oxLDL are recycled into the plasma membrane for a new round of internalization. Subsequently, oxLDL is delivered to the early endosome, late endosome, and lysosome successively for degradation[51]. Deubiquitylation of SRA1 reduces the internalization of the oxLDL-SRA1 complex. However, the fate of SRB1 carrying oxLDL and whether ubiquitylation of SRB1 affects its trafficking have not been elucidated. In this study, we revealed that RNF128-mediated ubiquitylation stabilized the SRB1 protein level by promoting its translocation to the membrane and preventing it from lysosomal degradation. RNF128 knockout does not affect SRB1 protein expression in the absence of oxLDL stimulation. However, with oxLDL stimulation, RNF128 knockout reduces both membrane SRB1 and total SRB1 levels. Lysosomal inhibitors can restore the total SRB1 levels degraded due to RNF128 knockout but do not influence the retention of membrane SRB1, which indicates that changes in membrane SRB1 are not driven by alterations in total SRB1 protein levels. The endocytic process for oxLDL phagocytosis includes clathrin-dependent endocytosis and recycling[13], where small GTPases of the Rab family accurately sort the proteins and lipids[44,52]. SRB1 colocalizes with Rab5 (early endosomal marker), Rab7 (late endosomal/lysosomal indicator), and Rab11 (referring to sorting/recycling endosome)[45,53], indicating that the Rab family controls SRB1 trafficking. Rab4 (fast recycling) and Rab11 (slow transit) are two Rab proteins associated with the recycling process[44]. Rab11 modulates endocytic cholesterol trafficking in an LDL-dependent or independent manner[54,55]. Huan Tao[56] discovered that intracellular macrophage SRB1 is localized to autophagosomes for cholesterol domains autophagy, which supported our findings that SRB1 could interact with Rab11 for recycling to cell surface rather than degradation by lysosomes.

Although SRB1 is degraded post-transcriptionally through the ubiquitin pathway[24], whether ubiquitylation affects SRB1 stabilization and translocation, as well as the exact modification site, remains unknown. K63-linked polyubiquitination regulates receptor internalization and sorting during endocytosis; coincidently, RNF128 localizes to endosomes[27]. Our study is the first to investigate that RNF128 could interact with SRB1 directly and catalyze K63-linked polyubiquitin chains of SRB1 at C-terminal lysine 478, resulting in stabilized membrane SRB1 and increased oxLDL uptake. When RNF128 was deficient, the combination between SRB1 and Rab11 weakened, suggesting that Rab11 was the critical link in the RNF128-mediated recycling of SRB1. Huang et al. have proven that residues in the C-terminus of SRB1 are critical for the uptake and transcytosis of LDL and modified LDL by endothelial cells[18], which is consistent with our findings.

RNF128 is a membrane-localized E3 ligase with a canonical sequence of 428 amino acids (isoform 1, as described in Uniprot: https://www.uniprot.org/uniprotkb/Q8TEB7/entry#sequences). The cytosolic zinc-binding RING finger domain possesses catalytic activity, and the luminal or extracellular PA domain captures transmembrane protein targets for ubiquitination[27]. RNF128 participates in the regulation of biological events; however, its specific role in the development of atherosclerosis and the underlying mechanisms remain unclear. Our study is the first to demonstrate that RNF128 accelerated atherogenesis. Based on the scRNA-seq data and experimental verification, we discovered that RNF128 was almost exclusively expressed in macrophages, and its expression was upregulated during atherogenesis. We developed mice with macrophage-specific RNF128 conditional knockout on an ApoE$^{-/-}$ background. We demonstrated that macrophage-specific deletion of RNF128 ameliorated diet-induced atherosclerosis by reducing lipid accumulation and lesion inflammation, which was also validated in LDLR-deficient mice. Regarding our mechanistic study, we investigated that RNF128 catalyzed K63-linked polyubiquitin chains of SRB1 at lysine 478 and promoted its Rab11-mediated recycling to the membrane, leading to increased oxLDL uptake, inflammation, and resultant foam cell formation (Graphical Abstract). Therefore, pharmacological inhibition of RNF128 may provide a potential therapeutic strategy for atherogenesis, and it is essential to explore the relationship between RNF128 variants in humans and atherosclerosis progression in the future.

Methods

Ethical regulation

All protocols were followed in accordance with the Ethical Committee of Ethics Committee of Qilu Hospital Shandong University (No. KYLL 2019(KS)-021).

Single-cell RNA sequencing (scRNA-seq) data re-analysis

FASTQ files of the atheroma of Ldlr-/- mice fed a Western diet (WD) for 0, 8, 16, and 26 weeks were obtained from the NCBI Gene Expression Omnibus database under the accession number GSE155513, which contained 28,816 cells[33]. Sample demultiplexing, barcode processing, and single-cell 3'gene counting by using the Cell Ranger pipeline (https://support.10xgenomics.com/single-cell-geneexpression/software/pipelines/latest/what-is-cell-ranger, version 5.0.1) and scRNA-seq data were aligned to the Ensembl genome GRCm38 reference genome.

https://doi.org/10.1038/s41467-025-57404-6

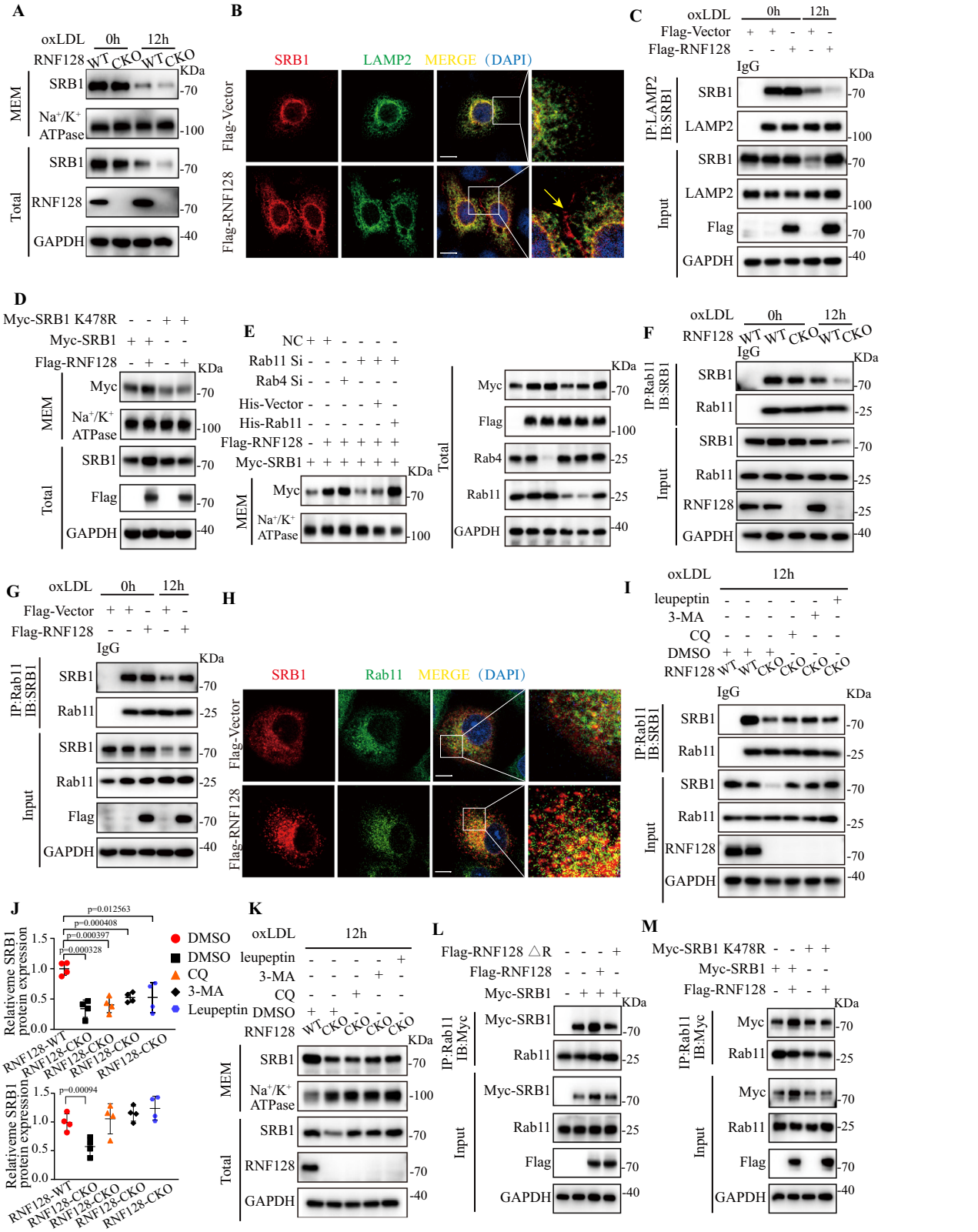

The Cell Ranger output was loaded into Seurat (version 3.1.1) for dimensionality reduction, clustering, and analysis. Data were integrated for batch effect removal, and batch correction was performed using Harmony. The Seurat software was used for dimensionality reduction and normalization. Principal component analysis was performed using normalized expression values, and the top ten principal components were selected for clustering and t-SNE (t-distributed stochastic neighbor embedding) analysis. A shared nearest neighbor (SNN) graph was used for clustering, and the Wilcoxon rank-sum test was performed to identify marker genes for different clusters. Finally, marker genes were selected that were expressed in more than 10% of the cells in a cluster with an average log (fold change) greater than 0.25.

Human coronary artery samples

Human coronary artery atheroma samples were obtained from autopsy specimens of body donors provided by the Red Cross Society

Fig. 6 | RNF128-mediated ubiquitination of SRB1 promotes its recycling to the membrane via Rab11. Plasma membrane (MEM) SRB1 refers to membrane SRB1 proteins purified using avidin from biotin-labeled membranes. Total SRB1 includes both membrane SRB1 and plasma SRB1 proteins, which are extracted from the whole lysate supernatant prior to avidin selection. **A** Western blotting analysis of total and MEM SRB1 in macrophages from RNF128-CKO and RNF128-WT mice with oxLDL stimulation. Sodium potassium ATPase (Na^+/K^+ ATPase) was used as a loading control for membrane protein ($n = 4$). **B** Laser confocal microscopy images of HeLa cells co-expressing either vector or Flag-tagged RNF128 with mCherry-tagged SRB1. Membrane SRB1 was marked by a yellow arrow ($n = 4$). Scale bar: 10 μm. **C** Western blotting analysis of indicated proteins immunoprecipitated with anti-LAMP2 or IgG antibody ($n = 4$). **D** Western blotting analysis of total and membrane proteins in HEK293T cells transfected with indicated plasmids ($n = 4$). **E** Western blotting analysis of total and membrane proteins in HEK293T cells ($n = 4$). **F** Western blotting analysis of indicated groups in macrophages immunoprecipitated with anti-Rab11 or rabbit IgG antibody ($n = 4$). **G** Western blotting analysis of indicated proteins in macrophages with Flag-RNF128 or vector overexpression immunoprecipitated with anti-Rab11 or rabbit IgG antibody ($n = 4$). **H** Confocal microscopy images of HeLa cells co-expressing either vector or Flag-tagged RNF128 with mCherry-SRB1 for 24 h. The colocalization of SRB1 and Rab11 was detected ($n = 4$). Scale bar: 10 μm. **I** Western blotting analysis of indicated proteins in macrophages immunoprecipitated with anti-Rab11 or rabbit IgG antibody ($n = 4$). **J** Quantification of SRB1 immunoprecipitated with anti-Rab11 antibody in **I** (upper) and total SRB1 protein of whole cell lysates in **I** (bottom) ($n = 4$). **K** Western blotting analysis of total and membrane proteins in macrophages incubated with DMSO, CQ, 3-MA, or leupeptin after oxLDL stimulation ($n = 4$). **L**, **M** Western blotting analysis of indicated groups in HEK293T cells immunoprecipitated with anti-Rab11 antibody ($n = 4$). The "n" represents the number of biologically independent samples. Data were presented as mean ± SD. Unpaired two-tailed Student's t-test was used for (**J**). ns not significant. Source data are provided as a Source Data file.

of Shandong Province, China. The Red Cross Society of Shandong Province has "written informed consent" from participants to collect the human samples, and we have the approval to use these samples. All body donors had coronary heart disease before accidental death. All protocols were approved by the Ethics Committee of the Qilu Hospital of Shandong University (No. KYLL 2019(KS)-021). The baseline characteristics of the human specimens used in the study are listed in Table S1. Consent to publish this information was obtained. Frozen sections of all samples were used for immunofluorescence staining[57]. For morphological classification for atherosclerotic lesions, the classification scheme for lesions proposed by the American Heart Association (AHA) was used. Early lesions are characterized by fatty dot or streak while in advanced lesions, intima is thickened by substantial repair-active fibrous tissue and then calcification appears[34].

Construction of macrophage-specific conditional RNF128 knockout mice

Macrophage-specific conditional RNF128 knockout (RNF128-CKO) mice on a C57BL/6J background were generated by crossing $RNF128^{fl/fl}$ mice (GemPharmatech Co., Ltd., Jiangsu, China) with $Lyz2^{cre}$ mice (GemPharmatech Co., Ltd.), referred to as $RNF128^{fl/fl}Lyz2^{cre}$ mice.

$RNF128^{fl/fl}$ mice were generated using the CRISPR/Cas9 technology by editing the *Rnf128* gene. According to the structure of the *Rnf128* gene, exon 2 of the Rnf128-201 (ENSMUST00000113026.1) transcript, which contains a 248 bp coding sequence, is recommended as the knockout region. Protein function was disrupted by the knockout. sgRNA was transcribed in vitro, and a donor vector was constructed. Cas9, sgRNA, and the donor vector were microinjected into fertilized eggs of C57BL/6J mice, which were then transplanted to obtain positive F0 mice, which was confirmed by PCR and sequencing. A stable F1 generation mouse model was obtained by mating positive F0 generation mice with C57BL/6J mice. $Lyz2^{cre}$ mice were generated using the CRISPR/Cas9 system.

The $RNF128^{fl/fl}Lyz2^{cre}$ mice were further crossed with $ApoE^{-/-}$ mice on a C57BL/6J background (GemPharmatech Co., Ltd.) to generate $ApoE^{-/-}RNF128^{fl/fl}Lyz2^{cre}$ mice to build the atherosclerotic model.

Mouse genotyping

The Mouse Direct PCR Kit (Bimake, B40015) was used for rapidly digesting mouse tissue to release intact genomic DNA that could be used directly as the template for PCR amplification (Buffer L: Protease Plus=50 μL: 1 μL for each sample). Then, the samples were put at 55 °C for 20 min followed by 95 °C for 5 min. The primer information is listed in Table S2. The PCR amplification components included 2 × Taq Master Mix (12.5 μL), double-distilled water (9.5 μL), primer forward (10 pmol/μL, 1 μL), primer reverse (10 pmol/μL, 1 μL), and template (100 ng/μL, 1 μL). The PCR program is shown below. Then, the DNA ladder was examined by DNA agarose gel electrophoresis.

Temperature	Time	Cycle
95 °C	5 min	1 ×
98 °C	30 s	20
65 °C (-0.5 °C /cycle)	30 s	
72 °C	45 s	
98 °C	30 s	20 ×
55 °C	30 s	
72 °C	45 s	
72 °C	5 min	1 ×
10 °C	hold	

Animal models

Early and advanced atherosclerotic plaques were obtained from male $ApoE^{-/-}$ mice (aged 6 weeks) (GemPharmatech Co., Ltd.) fed a WD (1.25% cholesterol, TP28521, Trophic Animal Feed High-tech Co., Ltd., Jiangsu, China) for different durations (8 and 20 weeks). The classification of lesions was defined by the duration of WD feeding ("early" and "advanced" lesions refer to WD feeding for 8 weeks and 20 weeks, respectively). Frozen plaque sections were used for immunofluorescence staining, and total protein extracted from whole aortas was used for Western blotting analysis.

Male or female $ApoE^{-/-}RNF128^{fl/fl}Lyz2^{cre}$ mice and their littermates, $ApoE^{-/-}RNF128^{fl/fl}$ mice (control group), were fed a WD for 20 weeks (aged 6 weeks). Low-density lipoprotein receptor (LDLR)-deficient mice were generated via adeno-associated virus (AAV)-proprotein convertase subtilisin/kexin type 9 (PCSK9) (WZ Biosciences Inc., Shandong, China) intravenous injection of $RNF128^{fl/fl}Lyz2^{cre}$ mice and $RNF128^{fl/fl}$ mice at 6 weeks old, followed by a WD for 20 weeks for both males and females. Then, mice were euthanized, and blood samples were collected from their cardiac apex. Tissue and plasma samples were collected for subsequent experiments. Randomization and blinding were adopted for the animal studies. All procedures were approved by the Ethical Committee of the Ethics Committee of Qilu Hospital Shandong University (No. KYLL 2019(KS)-021). All mice were on a C57BL/6J background and housed under a controlled environment (20 ± 2 °C, 12:12 h light/dark cycle) in the Animal Care Center of Qilu Hospital of Shandong University[36].

Animal randomization, blinding, and determination of group size

To avoid the underlying variables that may result in skewed data, a random number table was used to achieve randomization. First, all mice were assigned a number from 1 to n ordered by their weight.

https://doi.org/10.1038/s41467-025-57404-6

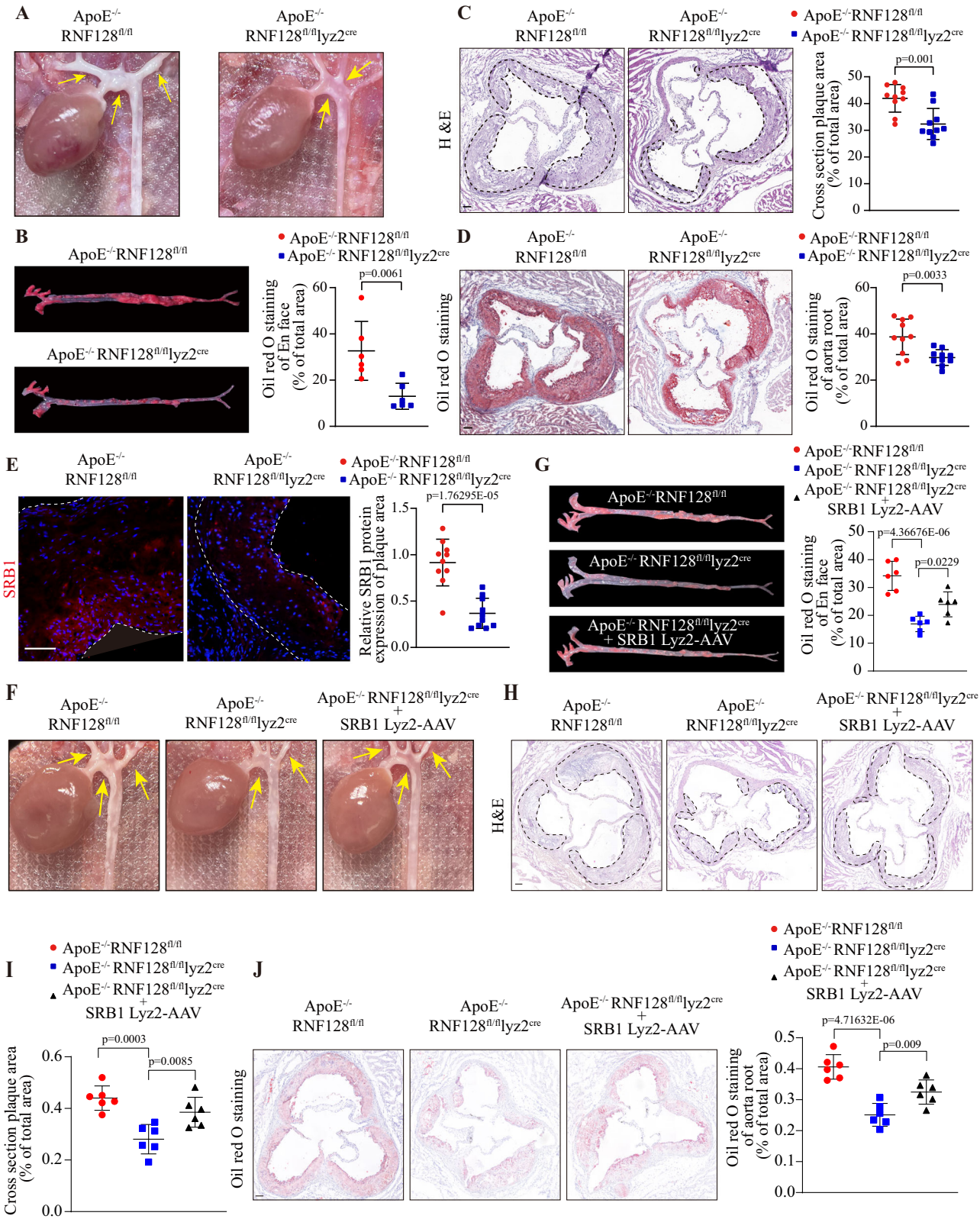

Then, we closed our eyes and randomly pointed to a spot on the random number table to obtain consecutive random numbers for the mice assignment. All selected random numbers ranged from small to large, and every consecutive 12 mice were chosen as one group. All data were collected and analyzed by two observers who were not aware of group assignment and treatment of mice to achieve animal blinding. No samples or animals were excluded from the data analysis.

The group size was determined according to our in vitro experiments. From Fig. 2A–D, we revealed that RNF128-deficient macrophages exhibited a ~50% decrease in foam cell formation as demonstrated with Oil red O staining as well as neutral lipid dyed with boron-dipyrromethene (BODIPY) in the presence of oxLDL. Therefore, we assumed that the mean of the experimental group is 0.6, the mean of the control group is 1.0, and the combined standard deviation is 0.255. Assuming type I error (α) and type II error (β) are 0.05 and

Fig. 7 | Macrophage-specific deletion of RNF128 ameliorates atherosclerosis (males). A Representative in situ images of the aortic arch with atherosclerotic plaques (yellow arrows) from ApoE$^{-/-}$RNF128$^{fl/fl}$Lyz2^{cre} mice and ApoE$^{-/-}$RNF128$^{fl/fl}$ mice fed a Western diet for 20 weeks ($n = 12$). **B** En face Oil red O staining of whole aortas (left) and data analysis (right). Plaque area was quantified as the percentage of lesion area/total surface area of the aorta ($n = 6$). **C** Hematoxylin-eosin (H&E) staining of cross sections at the aortic root (left) and data analysis (right). Atherosclerotic plaques were demarcated by black dashed lines ($n = 10$). Scale bar: 100 μm. **D** Oil red O staining of aortic root sections (left) and data analysis (right). Lesion size was quantified as the percentage of lesion area/lumen area ($n = 10$). Scale bar: 100 μm. **E** SRB1 protein identified by immunofluorescent staining in aortic root lesions (left) and data analysis (right). Atherosclerotic plaques were demarcated by white dashed lines ($n = 10$). Scale bar: 100 μm. **F** Representative in situ images of aortic arch with atherosclerotic plaques (yellow arrows) from ApoE$^{-/-}$RNF128$^{fl/fl}$Lyz2^{cre} mice, ApoE$^{-/-}$RNF128$^{fl/fl}$ mice, and ApoE$^{-/-}$RNF128$^{fl/fl}$Lyz2^{cre} + SRB1 Lyz2-AAV mice fed a Western diet for 20 weeks ($n = 6$). **G** En face Oil red O staining of whole aortas (left) and data analysis (right). Plaque area was quantified as the percentage of lesion area/total surface area of the aorta ($n = 6$). **H** Hematoxylin-eosin (H&E) staining of cross sections at the aortic root. Atherosclerotic plaques were demarcated by black dashed lines. Scale bar: 100 μm. **I** Data analysis of (H) ($n = 6$). **J** Oil red O staining of aortic root sections (left) and data analysis (right). Lesion size was quantified as the percentage of lesion area/lumen area ($n = 6$). Scale bar: 100 μm. Data were presented as mean ± SD. Normal distribution was tested by the Shapiro–Wilk method. Unpaired two-tailed Student's *t*-test was used for (**B**–**E**). The "*n*" represents the number of biologically independent samples. One-way ANOVA followed by the Dunnett post hoc test was used for the others. Source data are provided as a Source Data file.

0.10, respectively, and the ratio of sample size between the two groups is 1 (experimental group: control group), the sample size is 9 in each group. Considering 20% of samples dropout like accidental mouse death, a total of 12 samples are required in each group. Therefore, for the generation of atherosclerosis model, we enrolled 12 mice in each male or female mouse groups (male ApoE$^{-/-}$RNF128$^{fl/fl}$Lyz2^{cre} group, male ApoE$^{-/-}$RNF128$^{fl/fl}$ group, female ApoE$^{-/-}$RNF128$^{fl/fl}$Lyz2^{cre} group, and female ApoE$^{-/-}$RNF128$^{fl/fl}$ group). The group size of LDLR-deficient mice was the same as ApoE$^{-/-}$ mice.

Production of the polyclonal antibody against RNF128

Rabbit polyclonal antibodies against both human and mouse RNF128 were produced by ABclonal Technology Co., Ltd (Wuhan, China), which specifically targeted amino acids 136-402 of the RNF128 sequence. Antibodies were applied for Western blotting, immunofluorescent staining, and co-immunoprecipitation (Co-IP).

Quantification of whole-aorta atherosclerotic lesions in mice

After being fed a WD for 20 weeks, the mice were fasted for 12 h then euthanized. Blood was collected from the right atrium and then centrifuged at 3000×*g*, and 4 °C for 10 min before plasma was removed for subsequent testing. Representative in situ images were obtained before the heart and aorta were removed from the mice. Then these were isolated and fixed in 4% paraformaldehyde or stored at -80 °C. After fixation, the adventitias of the aortas were cleaned using an anatomical microscope for Oil Red O staining. An Oil Red O solution (0.5%) was prepared by dissolving Oil Red O powder (1320-06-5, Sigma-Aldrich, USA) in isopropyl alcohol and then diluting it with double-distilled water. Clean aortas were stained for 30 min followed by decolorization with 75% ethanol. Then en face pictures were taken and analyzed using Image-Pro Plus (IPP; Media Cybemetics, USA, 7.0) software. The plaque area was quantified as the proportion of the lesion area/total surface area of the aorta. Data analysis was performed by investigators blind to mouse genotype.

Quantification of atherosclerotic lesions in aortic root cross-sections

Hearts were dissected from the aortas, embedded in optimal cutting temperature compound (Sakura, USA) and cut into 6-μm-thick cross-sections for staining. After fixation, the slides were stained with Oil Red O solution for 15 min, followed by decolorization with 75% ethyl alcohol. After washing with phosphate-buffered saline (PBS), the slides were incubated with hematoxylin for 1 min and washed with PBS. The slides were also stained with hematoxylin and eosin (Solarbio, Beijing Solarbio Science & Technology, China) according to the manufactures' instructions. After mounting with gelatin glycerin (S2150, Solarbio) or neutral balsam (G8590, Solarbio), images were captured by scanning and measured using the IPP software. Then lesion size was quantified as the proportion of the lesion area/lumen area. Data analysis was performed by investigators blind to mouse genotype.

Quantification of lipid levels

Circulating blood was collected from mice in a test tube coated with heparin. After blood centrifugation at 3000×*g* and 4 °C for 10 min, plasma was collected and stored at −80 °C. Plasma cholesterol and lipid levels, including triglyceride, total cholesterol (CHO), LDL cholesterol, and high-density lipoprotein (HDL) cholesterol levels were measured (Servicebio Technology Co., Wuhan, China). Data analysis was performed by investigators blind to mouse genotype.

Total protein extraction of whole aortas

Total protein from whole aortas was extracted using a Minute™ Total Protein Extraction Kit (SD-001/SN-002, Invent, USA). The protein extraction filter cartridge was pitted in the collection tube and pre-chilled on ice prior to the extraction process. Then, 15–30 mg of aorta tissue pre-frozen at −80 °C was placed in the filter. A plastic rod was used to grind and twist the tissue ~60 times. After that, 200 μL of denaturing Cell Lysis buffer was added, and the tissue was again ground 60 times. The filter was capped and incubated at room temperature for 2 min before centrifugation at 13,000×*g*, and 4 °C for 2 min, and the supernatant containing protein was collected. The loading buffer (TransGen Biotech, Beijing, China) was added, followed by incubation at 99 °C for 5 min and Western blotting analysis.

Immunofluorescent (IF) staining for tissue cross-sections

Frozen cross-sectional slides of human aorta samples and mouse aortic roots were placed at room temperature for temperature recovery. They were then incubated with 3% H_2O_2 for 10 min to inhibit endogenous peroxidase and next permeabilized using 0.4% Triton X-100 (T8200, Solarbio) dissolved in PBS for 10 min at room temperature. Next, the slides were blocked with 10% donkey serum for 1 h at room temperature. Afterward, primary antibodies, including rat monoclonal antibody against monocyte + macrophage (anti-MOMA-2), rabbit monoclonal antibody against scavenging receptor SRB1, and rabbit polyclonal antibody against RNF128 (1:50), were incubated with the slides at 4 °C overnight. The following day, the slides were incubated with the corresponding fluoresce secondary antibodies, including donkey anti-rabbit IgG H&L (Alexa Fluor® 594) (ab150064, Abcam, UK) and donkey anti-rat IgG H&L (Alexa Fluor® 488) (ab150153, Abcam) for 2 h. Sections reacting with non-immune IgG (1:50, ab182931, Abcam; 1:50, 30000-0-AP, Proteintech), as well as secondary antibodies, were used as negative controls. After washing with PBS, the slides were stained with DAPI (ab104139, Abcam) for fluorescence imaging using an upright electron microscope (DS-Ri2, Nikon, Japan).

Immunohistochemical staining of tissue cross-sections

Frozen cross-sectional slides of mouse aortic roots were placed at room temperature for temperature recovery. They were then incubated with 3% H_2O_2 for 10 min to inhibit endogenous peroxidases. Next, the slides were blocked with 5% goat serum for 1 h at room temperature. Afterward, primary antibodies, including rabbit

polyclonal antibody against tumor necrosis factor α (TNFα), rabbit monoclonal antibody against interleukin-6 (IL6), and rabbit polyclonal antibody against interleukin-1β (IL1β) were incubated with the slides at 4 °C overnight. The following day, the slides were incubated with horseradish peroxidase (HRP)-conjugated goat anti-rabbit IgG (PV-9001, ZSJB-Bio in Beijing, China) for 1 h at room temperature. Sections reacting with non-immune IgG, as well as secondary antibodies, were used as negative controls. After PBS-washing, slides were stained using a DAB kit (ZSGB-Bio). Nuclei were counterstained with hematoxylin. Images were captured using an upright electron microscope. The sections that reacted with non-immune IgG and secondary antibodies were used as negative controls.

In vivo oxLDL uptake

To confirm the function of SRB1 for lipid uptake in vivo, adeno-associated viruses encoding a macrophage-specific short hairpin RNA (shRNA) were constructed based on the pAV-Lyz2-shRNA-CMV-GFP vector, and intravenously administered to $ApoE^{-/-}$ male mice aged 6 weeks following a WD feeding for 15 weeks. Control mice were treated with AAV-Lyz2-shRNA-control, while mice of the SRB1 Lyz2-shRNA group were injected with AAV-Lyz2-shRNA-SRB1 (sequence: GCTCAAGAATGTCCGCATA) for the downregulation of SRB1 in macrophages.

To evaluate oxLDL uptake in vivo, following receipt of the atherogenic diet, mice were injected retro-orbitally with Dil-oxLDL (100 μg) for an hour, and then, mice were anesthetized and perfused with ice-cold PBS. Similarly sized plaques were isolated from the thoracic aorta subjected to Hoechst staining (5 μg/ml, Abcam, ab228550) at 4 °C for 30 min to identify nuclei. After washing three times, the fluorescence confocal microscopy was performed on the luminal surface using a 20 × objective and a Zeiss LSM900 microscope. These methods were adapted from approaches employed to visualize LDL transport across the endothelial monolayer in vivo[17].

Cell culture

Primary peritoneal macrophages were isolated from $RNF128^{fl/fl}Lyz2^{cre}$ and $RNF128^{fl/fl}$ male mice at 8 weeks old. First, the mice were intraperitoneally injected with 1 mL of 5% sterile starch and were euthanized after 3 days for cell extraction. The abdomen of each mouse was soaked in 75% alcohol, and the lower abdomen was incised along the midline. Then medium was then injected and withdrawn to extract peritoneal exudate cells. After centrifugation at 800 rpm at room temperature for 5 min, the supernatant was discarded and the cells were resuspended in complete Dulbecco's modified Eagle's medium (DMEM; C11995500BT, Gibco, USA) supplemented with 10% heat-inactivated fetal bovine serum (10099-141, Gibco) and 1% penicillin-streptomycin (15140122, Gibco). Cells were counted and incubated in a humidified atmosphere of 5% CO_2 at 37 °C for 6 h, then non-adherent cells were removed by gently washing with warm PBS. The adherent macrophages were incubated in complete DMEM.

The mouse leukemic monocyte-macrophage cell line (RAW264.7, Oricell, passage No. 5 to passage No. 15) was cultured in DMEM supplemented with 10% heat-inactivated fetal bovine serum (ExCell Bio, Shanghai, China, Cat# FND500). The human monocyte leukemia cell line (THP-1, KeyGene BioTech, passage No. 5 to passage No. 10) was treated with phorbol 12-myristate 13-acetate (PMA, 100 nM; HY-18739, MCE, China) for 24 h for transformation into adherent macrophages. Human HEK293T cells and HeLa cells were obtained from KeyGene BioTech (China) and cultured in complete DMEM. Macrophages were treated with oxidized LDL (oxLDL; Peking Union-Biololgy Co.Ltd, Bejing, China) or cycloheximide (CHX; HY-12320, MCE).

SRB1 stably knockout RAW264.7 cell line generation

SRB1 stably knockout RAW264.7 cell line was generated using the CRISPR/Cas9 technique. First, cells were transfected with LentiCRISPR v2-Puro vector encoding Scarb1 sgRNA (sequence: GGTCCACGCTCCCGGACTAC). Subsequently, the transfected cells were subjected to puromycin selection, and the efficiency of knockout in transfected cells was confirmed by PCR.

Total cell protein extraction

Cells were lysed using Cell Lysis (C2978, Sigma-Aldrich, USA) supplemented with a protease inhibitor cocktail (1:100, CW2200S, CWBIO in Beijing, China). After centrifuging at 13,000×*g* and 4 °C for 15 min, the supernatant was collected, and the protein concentration was measured using a BCA Protein Assay Kit (23227; Thermo Fisher Scientific, USA). Then, loading buffer was added, followed by incubation at 99 °C for 5 min and Western blotting analysis.

Membrane cell protein preparation

After oxLDL treatment, cells were washed twice with cold PBS, then incubated with sulfo-NHS-SS-biotin (0.5 mg/mL; PG82077, Thermo Fisher Scientific) and gently shaken for 30 min at 4 °C. The reaction was terminated with glycine. Then cells were lysed using Cell Lysis (1 mL per sample) containing protease inhibitor and centrifuged at 13,000×*g* and 4 °C for 10 min. The supernatant was collected, and the protein concentration was tested as described above. The supernatant fraction represented the total protein fraction, and 100 μL was removed from the supernatant to treat it as the total protein. Then the rest of the supernatant (900 μL) was incubated with Pierce NeutrAvidin agarose beads (40 μL; 29200, Thermo Fisher Scientific), which combined with the sulfo-NHS-SS-biotin-attached membrane protein at 4 °C overnight. After washing with protease inhibitor-containing PBS four times, agarose beads were boiled with 2× loading buffer at 99 °C for 5 min, and membrane proteins dissociated from the beads into the supernatant. The membrane and total protein levels were measured by using Western blotting.

Western blotting analysis

Western blotting was performed according to the standard protocol[58]. Briefly, proteins extracted from tissues or cells were separated by 10% sodium dodecyl sulfate (SDS)-PAGE (Bio-Rad Laboratories, USA) and then transferred to 0.45 or 0.22 μm PVDF membranes (ISEQ00010/IPVH00010, Millipore, USA). After incubation with 5% bovine serum albumin, transferred blots were incubated with primary antibodies (listed in Table S3) overnight at 4 °C. The next day, blots were incubated with HRP-conjugated anti-rabbit or anti-mouse secondary antibodies at room temperature for 1 h. Blot images were captured using a chemiluminescent reagent (WBKLS0500, Millipore, USA) and a luminescent imaging instrument (Amersham Imager 680, GE, USA). Finally, the Gray values detected using ImageJ software (Version 1.54, National Institutes of Health, NIH) were used for quantification. Total protein levels were normalized to the GAPDH levels.

Total RNA extraction and quantitative RT-PCR assay

Total RNA was extracted from mouse macrophages using a Total RNA Extraction Kit (220011, Fastagen in Shanghai, China) according to the manufacturer's protocols. The total RNA was then reverse transcribed using a PrimeScript RT reagent kit, including a gDNA eraser (RR047A, TaKaRa, Japan). Synthesis was performed by subjecting each sample to 2 min at 42 °C, 15 min at 37 °C to allow for reverse transcription, and 5 s at 85 °C for reverse transcriptase inactivation.

The obtained cDNA samples were subjected to quantitative PCR for *Tnfα*, *iNos*, *Il6*, and *Il1β* detection using the LightCycler® 480 SYBR® Green I Master (04887352001, Roche, Switzerland) for the Light Cycler480 instrument (Roche Light Cycler480). The SYBR reaction components included DNA template (2 μL), primer forward (10 μM, 0.5 μL), primer reverse (10 μM, 0.5 μL), SYBR (10 μL), and double-distilled water (7 μL). The program was as shown below. The level of

β-actin was used for data normalization, and the $2^{-\Delta\Delta Ct}$ method was used for calculation. The primer sequences are listed in Table S4.

Temperature	Time	Cycle
95 °C	10 min	1 ×
95 °C	15 s	40 ×
55 °C	15 s	
72 °C	20 s	

Co-IP analysis

Interactions were validated in HEK293T cells transfected with exogenous plasmids expressing Green fluorescent protein (GFP)-tagged RNF128, Flag-tagged ABCG1, SRA1, SRB1, CD36 as well as CD68, and others. After transfection for 24 h, the cells were lysed using Cell Lysis with a protease inhibitor cocktail. After centrifugation for 15 min at 13,000×*g* and 4 °C, supernatant was collected, with 100 μL of supernatant usually being removed to be treated as the "Input". Then, the remaining supernatant was incubated with agarose immunoprecipitation beads for tag combination at 4 °C overnight on a rotary mixer. The beads were then washed five times with radioimmunoprecipitation assay buffer (P0013c, Beyotime Biotechnology, China). Precipitated proteins were separated from beads after incubation at 99 °C for 5 min with 2 × loading buffer. Then immunoprecipitated proteins were subjected to Western blotting.

Endogenous Co-IP between RNF128 and SRB1 was performed on macrophages to verify their combination in response to oxLDL stimulation. The Co-IP protocol was similar to that used for the exogenous interaction test described above. After supernatant preparation, corresponding antibodies were added to combine with endogenous protein for incubation at 4 °C for 1 h. Then, protein A/G Plus Agarose (sc-2003, Santa Cruz Biotechnology, USA) was used for antibody-combination at 4 °C overnight with gentle mixing. Normal rabbit IgG (2729S, Cell Signaling Technology, Danvers, MA, USA) was used as a negative control. To avoid light chain and heavy chain for different antibodies, different secondary antibodies were used, which have been listed in Table S3.

Ubiquitination analysis

Ubiquitination assays were performed using HEK293T cells transfected with exogenous plasmids expressing HA-tagged ubiquitin (WT), HA-ubiquitin (K48), HA-ubiquitin (K63), Flag-tagged RNF128 (including its mutants), or Myc-tagged SRB1 (including its mutants). After transfection for 24 h, the cells were lysed using Cell Lysis with a protease inhibitor cocktail. The lysates were immediately boiled for 10 min in the presence of 1% SDS, followed by dilution with lysis buffer until the SDS concentration reached 0.1%. Cell extracts were immunoprecipitated with Myc-specific beads to enrich the SRB1 protein combined with ubiquitin chains. Precipitated proteins were analyzed by immunoblotting with an anti-HA antibody[59].

Endogenous SRB1 ubiquitination was also detected in macrophages following oxLDL stimulation. The extraction of macrophages was immunoprecipitated using an anti-SRB1 antibody and subjected to Western blotting analysis with anti-ubiquitin (Ub), anti-ubiquitin (K48), or anti-ubiquitin(K63) antibodies.

Co-IP and ubiquitination assay in vitro

The purified recombinant proteins were used for in vitro experiments. Binding assays were performed by mixing GST-RNF128 (1 μg, H00079589-P01, Abnova) or GST-control (1 μg, RP02000, ABclonal) with His-SRB1 (1 μg, 11069-H08H, Sino Biological Inc., Beijing, China) together at 4 °C for 1 h, and the proteins were immunoprecipitation with a GST antibody at 4 °C overnight, followed by Western blotting analysis using an anti-His antibody. For ubiquitination, a ubiquitination kit (Boston Biochem) was used according to the manufacturer's instructions.

Plasmids construction

Plasmids encoding wild-type RNF128, SRB1, ABCG1, ABCA1, SRA1, CD36, CD68, and control vectors were purchased from GeneCopoeia, Inc. Mutation generation was based on wild-type plasmids used as templates. The KOD-Plus-Mutagenesis Kit was used for mutation instruction (A3634K, TOYOBO Life Science, Japan). The sequences of all the constructs were verified by DNA sequencing (BGI, China).

Plasmids and siRNA transfection

For plasmids transfection, empty vectors were used for completion so that the amounts of plasmids among groups kept the same and the transfection efficiency would not be affected by different amounts of plasmids. Plasmids were transiently transfected into HEK293T cells or HeLa cells using Lipofectamine 3000 reagent (L3000015, Invitrogen, USA) according to the manufacturer's protocols. Briefly, cells were seeded to be 70–90% confluent at transfection. Lipofectamine 3000 reagent was diluted in Opti-MEM medium (31985-070, Gibco, USA). Then, a master mix of plasmids was prepared by diluting plasmids in Opti-MEM medium with the addition of P3000 reagent (plasmids: P3000 reagent = 1: 1 ratio). After incubation for 5 min, diluted plasmids were added to each tube of diluted Lipofectamine 3000 reagent (1: 1 ratio). After incubation for 15 min, a plasmids-lipid complex was added to the cells. The jetOPTIMUS transfection reagent (Polyplus, 117-15) was used for the transfection of RAW264.7 cells. Cells were seeded to be 60–80% confluent at transfection. We diluted 2 μg of DNA in 50 μL of jetOPTIMUS buffer. Then, 2 μg of jetOPTIMUS reagent was added. After incubation for 10 min at room temperature, the transfection mix was added to the cells.

The Lipofectamine RNAiMAX reagent (56532, Invitrogen) was used for siRNA transfection of macrophages and HEK293T cells. Briefly, cells were seeded to be 80-90% confluent at transfection. Lipofectamine RNAiMAX reagent and siRNA were diluted in Opti-MEM medium, separately. After incubation for 5 min, diluted siRNA and the same amount of negative control siRNA were added to the diluted Lipofectamine RNAiMAX reagent. After incubation for 10 min, siRNA-lipid complex was added to cells. After transfection with plasmids or siRNA for 24 h, the cells could be treated with further processing, then lysed for protein collection. Target sequences of the siRNAs used in this study are listed in Table S5. All siRNAs were purchased from RiboBio (Guangzhou, China).

Adenovirus overexpression in macrophages

Adenovirus carrying C-terminal Flag-RNF128 (Flag-RNF128), a mutant of C-terminal Flag-RNF128 (Flag-RNF128 ΔR), and C-terminal Flag-SRB1 (Flag-SRB1) were obtained from BioSune Biotechnology (Shanghai, China). Macrophage infection was performed according to the multiplicity of infection (MOI) using polybrene (BioSune Biotechnology) for 12 h. For adenovirus infection, Falg-tagged vectors were used for completion so that the infection efficiency would not be affected by different amounts of adenovirus. Then, the supernatant was replaced with fresh complete DMEM for 48 h prior to the next treatment.

Laser confocal microscopy and immunofluorescence staining of cells

Cells were seeded on climbing slices for the next staining. Plasmids expressing GFP-tagged RNF128 and mCherry-tagged SRB1 with autofluorescence were co-transfected into HEK293T cells for 24 h. The cells were then fixed with 4% paraformaldehyde, and the nuclei were counterstained with DAPI. For HEK293T cells transfected with Myc-SRB1 without autofluorescence or macrophages, antibodies were used.

After fixation, the cell membranes were permeabilized with 0.1% Triton X-100 for 5 min, and then 10% goat serum was used for blocking. Then, cells were incubated using the indicated primary antibodies at 4 °C overnight. On the next day, the corresponding fluorescent secondary antibodies were used for multiple signaling cascades. DAPI was used for nuclei staining and mounting. Samples incubated with IgG and secondary antibodies were used as negative controls. Images were captured using a laser confocal microscope or upright electron microscope.

Oil Red O staining of foam cells

Macrophages were incubated with 75 μg/mL oxLDL for 24 h and then fixed with 4% paraformaldehyde for 10 min. Before Oil Red O staining, the cells were incubated with 60% isopropanol for 5 min. They were then incubated with 0.5% Oil Red O solution for 30 to 60 min, until the red lipid droplets were visible under a microscope. After washing with double-distilled water, the nuclei were stained with hematoxylin and mounted with gelatin glycerin. Images were captured by scanning and measured using IPP software. For quantification, we selected fields of the same size with similar cell densities, and calculated the optical density value using IPP. We took the average optical density values of different samples in the control group for normalization, and then the optical density values of all samples were compared with the normalized value to obtain the relative values (relative Oil Red O staining) for analysis.

BODIPY staining of lipids

BODIPY™ 493/504 was used to stain for neutral lipids (790389, Sigma-Aldrich, USA)[60]. The cells were seeded onto climbing slices and incubated with oxLDL at the indicated time points. After washing with PBS three times, the cells were stained with BODIPY (1 μg/mL dissolved in DMSO) for 30 min at room temperature. After washing with PBS, the nuclei were stained with DAPI. Images were captured using an upright electron microscope, and fluorescence intensity (green color) was measured using IPP software. The quantification method is the same as the quantification of oil red o staining.

Total cholesterol assay of macrophages

The level of total cholesterol in macrophages in response to oxLDL was measured using a Tissue Total Cholesterol Assay Kit (E1005, Applygen Technologies Inc. in Beijing, China) according to the manufacturer's protocol[61].

Lipid uptake assays

Macrophages and HeLa cells transfected with Myc-SRB1 plasmids were incubated with Dil-oxLDL (20 μg/mL; Yiyuan, Guangzhou, China) at 37 °C for 6 h. After fixation and PBS-washing, the nuclei were stained with DAPI. Images were captured using a laser confocal microscope or upright electron microscope. Fluorescence intensity (red color) was measured using IPP software. The quantification method is the same as the quantification of Oil Red O staining.

Cholesterol efflux assay of macrophages

After incubation with oxLDL for 12 h, the macrophage medium was refreshed for subsequent experiments. Macrophages were treated with Bodipy-labeled cholesterol (5 μg/mL) for 24 h. The medium was replaced with fresh serum-free DMEM, and different efflux acceptors, such as recombinant HDL (50 μg/mL) or ApoAI (20 μg/mL), were added for incubation at 37 °C for 6 h. After incubation, the medium was collected and centrifuged at 12,000×*g* at 4 °C for 2 min. In addition to the medium, cells were dissolved in 0.1 N NaOH overnight to determine the protein levels and radioactivity. The levels of cholesterol in the medium and dissolved from cells were determined through spectrometry. The rate of cholesterol efflux was calculated as (amount in medium/amount in medium and cell lysate) × 100%[62].

Statistical analysis

Statistical analysis was performed using SPSS 23.0 (SPSS Inc., Chicago, 20 IL, USA) and GraphPad Prism 8 software (GraphPad Software, San Diego, CA, USA). All data are expressed as mean ± standard deviation (SD). The number of replicates is indicated in the figure legend, and independent replicates were performed for each experiment.

The Shapiro–Wilk test was used to evaluate the normality of the data distribution and the Levene test was used for homogeneity of variance test. For normally distributed data with homogeneity of variance, the statistical difference between two groups was determined by the unpaired, two-tailed Student's *t*-tests, while a one-way ANOVA test was used for data where multiple groups existed with only one variable, followed by Dunnett's or Tukey's post hoc tests. Comparisons among multiple groups with two or more variables were performed using two-way ANOVA, followed by Tukey's or Sidak's post hoc tests. To analyze the non-normally distributed data or data with different variances, a nonparametric test was used. The Mann–Whitney test was used for between-group comparison, and the Kruskal–Wallis test followed by a Dunn test, was used for multiple-group comparisons. Adjusted *P* values were provided in case of multiple-group comparisons. If the *p* value was less than 0.05, the comparison was considered to be statistically significant. Each symbol in the statistical profile represents the number of independent repeats, patients, or mice. The statistical tests resulting in the data shown in each figure are listed in the corresponding figure legends.

Reporting summary

Further information on research design is available in the Nature Portfolio Reporting Summary linked to this article.

Data availability

Data supporting the findings of this study are available in the article and its Supplementary information. Source data are provided as Source Data file and may be obtained from the corresponding authors upon request. FASTQ files were obtained from the NCBI Gene Expression Omnibus database under the accession number GSE155513. Source data are provided with this paper.

References

1. Libby, P. The changing landscape of atherosclerosis. *Nature* **592**, 524–533 (2021).
2. Wang, J. K. et al. Ablation of plasma prekallikrein decreases low-density lipoprotein cholesterol by stabilizing low-density lipoprotein receptor and protects against atherosclerosis. *Circulation* **145**, 675–687 (2022).
3. Brophy, M. L. et al. Myeloid-specific deletion of Epsins 1 and 2 reduces atherosclerosis by preventing LRP-1 downregulation. *Circ. Res.* **124**, e6–e19 (2019).
4. Collaborators, G.B.D.C.o.D. Global, regional, and national age-sex-specific mortality for 282 causes of death in 195 countries and territories, 1980-2017: a systematic analysis for the Global Burden of Disease Study 2017. *Lancet* **392**, 1736–1788 (2018).
5. Robinson, J. G. & Gidding, S. S. Curing atherosclerosis should be the next major cardiovascular prevention goal. *J Am. Coll. Cardiol.* **63**, 2779–2785 (2014).
6. Tsao, C. W. et al. Heart disease and stroke statistics-2022 update: a report from the American Heart Association. *Circulation* **145**, e153–e639 (2022).
7. Zhang, X. et al. High-protein diets increase cardiovascular risk by activating macrophage mTOR to suppress mitophagy. *Nat. Metab.* **2**, 110–125 (2020).
8. Tomas, L., Prica, F. & Schulz, C. Trafficking of mononuclear phagocytes in healthy arteries and atherosclerosis. *Front. Immunol.* **12**, 718432 (2021).

9. von Ehr, A., Bode, C. & Hilgendorf, I. Macrophages in atheromatous plaque developmental stages. *Front. Cardiovasc. Med.* **9**, 865367 (2022).
10. Farahi, L., Sinha, S. K. & Lusis, A. J. Roles of macrophages in atherogenesis. *Front. Pharmacol.* **12**, 785220 (2021).
11. Chen, W. et al. Macrophage-targeted nanomedicine for the diagnosis and treatment of atherosclerosis. *Nat. Rev. Cardiol.* **19**, 228–249 (2022).
12. Moore, K. J., Sheedy, F. J. & Fisher, E. A. Macrophages in atherosclerosis: a dynamic balance. *Nat. Rev. Immunol.* **13**, 709–721 (2013).
13. Wang, B. et al. Disruption of USP9X in macrophages promotes foam cell formation and atherosclerosis. *J. Clin. Invest.* **132**, e154217 (2022).
14. Shen, W. J., Azhar, S. & Kraemer, F. B. SR-B1: a unique multifunctional receptor for cholesterol influx and efflux. *Annu. Rev. Physiol.* **80**, 95–116 (2018).
15. Huby, T. & Le Goff, W. Macrophage SR-B1 in atherosclerotic cardiovascular disease. *Curr. Opin. Lipidol.* **33**, 167–174 (2022).
16. Gillotte-Taylor, K., Boullier, A., Witztum, J. L., Steinberg, D. & Quehenberger, O. Scavenger receptor class B type I as a receptor for oxidized low density lipoprotein. *J. Lipid Res.* **42**, 1474–1482 (2001).
17. Huang, L. Z. et al. SR-B1 drives endothelial cell LDL transcytosis via DOCK4 to promote atherosclerosis. *Nature* **569**, 565–569 (2019).
18. Armstrong, S. M. et al. A novel assay uncovers an unexpected role for SR-BI in LDL transcytosis. *Cardiovasc. Res.* **108**, 268–277 (2015).
19. Sun, B. et al. Distinct mechanisms for OxLDL uptake and cellular trafficking by class B scavenger receptors CD36 and SR-BI. *J. Lipid Res.* **48**, 2560–2570 (2007).
20. de Villiers, W. J. S. & Smart, E. J. Macrophage scavenger receptors and foam cell formation. *J. Leukoc. Biol.* **66**, 740–746 (1999).
21. Maxfield, F. R. Role of endosomes and lysosomes in human disease. *Cold Spring Harb. Perspect. Biol.* **6**, 15 (2014).
22. Boullier, A. et al. Scavenger receptors, oxidized LDL, and atherosclerosis. *Ann. N. Y. Acad. Sci.* **947**, 214–223 (2001).
23. Lu, X. et al. NHERF1 and NHERF2 regulation of SR-B1 stability via ubiquitination and proteasome degradation. *Biochem. Biophys. Res. Commun.* **490**, 1168–1175 (2017).
24. Foot, N., Henshall, T. & Kumar, S. Ubiquitination and the regulation of membrane proteins. *Physiol. Rev.* **97**, 253–281 (2017).
25. Hong, C. et al. The E3 ubiquitin ligase IDOL induces the degradation of the low density lipoprotein receptor family members VLDLR and ApoER2. *J. Biol. Chem.* **285**, 19720–19726 (2010).
26. Chandra, D. et al. The SCFFBXO3 ubiquitin E3 ligase regulates inflammation in atherosclerosis. *J. Mol. Cell Cardiol.* **126**, 50–59 (2019).
27. Whiting, C. C., Su, L. L., Lin, J. T. & Fathman, C. G. GRAIL: a unique mediator of CD4 T-lymphocyte unresponsiveness. *FEBS J.* **278**, 47–58 (2011).
28. Anandasabapathy, N. et al. GRAIL: an E3 ubiquitin ligase that inhibits cytokine gene transcription is expressed in anergic CD4(+) T cells. *Immunity* **18**, 535–547 (2003).
29. Song, G. H. et al. E3 ubiquitin ligase RNF128 promotes innate antiviral immunity through K63-linked ubiquitination of TBK1. *Nat. Immunol.* **17**, 1342–1351 (2016).
30. Ray, D. et al. Isoforms of RNF128 regulate the stability of mutant P53 in Barrett's esophageal cells. *Gastroenterology* **158**, 583–597 (2020).
31. Liu, P. Y. et al. E3 ubiquitin ligase Grail promotes hepatic steatosis through Sirt1 inhibition. *Cell Death Dis.* **12**, 15 (2021).
32. Liu, P. Y. et al. Grail is involved in adipocyte differentiation and diet-induced obesity. *Cell Death Dis.* **9**, 12 (2018).
33. Pan, H. Z. et al. Single-cell genomics reveals a novel cell state during smooth muscle cell phenotypic switching and potential therapeutic targets for atherosclerosis in mouse and human. *Circulation* **142**, 2060–2075 (2020).
34. Stary, H. C. et al. A definition of advanced types of atherosclerotic lesions and a histological classification of atherosclerosis. A report from the Committee on Vascular Lesions of the Council on Arteriosclerosis, American Heart Association. *Arterioscler. Thromb. Vasc. Biol.* **15**, 1512–1531 (1995).
35. Yuan, Y., Li, P. & Ye, J. Lipid homeostasis and the formation of macrophage-derived foam cells in atherosclerosis. *Protein Cell* **3**, 173–181 (2012).
36. Liu, Z. Y. et al. Macrophage liver kinase B1 inhibits foam cell formation and atherosclerosis. *Circ. Res.* **121**, 1047–1057 (2017).
37. Wang, L. G., Miller, A. & Kendall, D. A. Signal peptide determinants of SecA binding and stimulation of ATPase activity. *J. Biol. Chem.* **275**, 10154–10159 (2000).
38. Schatz, G. & Dobberstein, B. Common principles of protein translocation across membranes. *Science* **271**, 1519–1526 (1996).
39. Lineberry, N., Su, L., Soares, L. & Fathman, C. G. The single subunit transmembrane E3 ligase gene related to anergy in lymphocytes (GRAIL) captures and then ubiquitinates transmembrane proteins across the cell membrane. *J. Biol. Chem.* **283**, 28497–28505 (2008).
40. Dikic, I. Proteasomal and autophagic degradation systems. *Ann. Rev. Biochem.* **86**, 193–224 (2017).
41. Borchers, A. G. M. et al. The E3 ubiquitin ligase GREUL1 anteriorizes ectoderm during Xenopus development. *Dev. Biol.* **251**, 395–408 (2002).
42. Takahashi, M. et al. Cholesterol controls lipid endocytosis through Rab11. *Mol. Biol. Cell* **18**, 2667–2677 (2007).
43. Wang, F. F., Chen, X. Q., Zhang, X. Q. & Ma, L. Phosphorylation state of mu-opioid receptor determines the alternative recycling of receptor via Rab4 or Rab11 pathway. *Mol. Endocrinol.* **22**, 1881–1892 (2008).
44. Soennichsen, B., De Renzis, S., Nielsen, E., Rietdorf, J. & Zerial, M. Distinct membrane domains on endosomes in the recycling pathway visualized by multicolor imaging of Rab4, Rab5, and Rab11. *J. Cell Biol.* **149**, 901–913 (2000).
45. Ahras, M., Naing, T. & McPherson, R. Scavenger receptor class B type I localizes to a late endosomal compartment. *J. Lipid Res.* **49**, 1569–1576 (2008).
46. Neculai, D. et al. Structure of LIMP-2 provides functional insights with implications for SR-BI and CD36. *Nature* **504**, 172–176 (2013).
47. Rahaman, S. O. et al. A CD36-dependent signaling cascade is necessary for macrophage foam cell formation. *Cell Metab.* **4**, 211–221 (2006).
48. Chinetti, G. et al. CLA-1/SR-BI is expressed in atherosclerotic lesion macrophages and regulated by activators of peroxisome proliferator-activated receptors. *Circulation* **101**, 2411–2417 (2000).
49. Kzhyshkowska, J., Neyen, C. & Gordon, S. Role of macrophage scavenger receptors in atherosclerosis. *Immunobiology* **217**, 492–502 (2012).
50. Rigotti, A., Miettinen, H. E. & Krieger, M. The role of the high-density lipoprotein receptor SR-BI in the lipid metabolism of endocrine and other tissues. *Endocr. Rev.* **24**, 357–387 (2003).
51. Stangl, H., Cao, G. Q., Wyne, K. L. & Hobbs, H. H. Scavenger receptor, class B, type I-dependent stimulation of cholesterol esterification by high density lipoproteins, low density lipoproteins, and nonlipoprotein cholesterol. *J. Biol. Chem.* **273**, 31002–31008 (1998).
52. Lakadamyali, M., Rust, M. J. & Zhuang, X. W. Ligands for clathrin-mediated endocytosis are differentially sorted into distinct populations of early endosomes. *Cell* **124**, 997–1009 (2006).
53. Jager, S. et al. Role for Rab7 in maturation of late autophagic vacuoles. *J. Cell Sci.* **117**, 4837–4848 (2004).
54. Hu, J. J. et al. Alteration in Rab11-mediated endocytic trafficking of LDL receptor contributes to angiotensin II-induced cholesterol accumulation and injury in podocytes. *Cell Prolif.* **55**, 11 (2022).

55. Holtta-Vuori, M., Tanhuanpaa, K., Mobius, W., Somerharju, P. & Ikonen, E. Modulation of cellular cholesterol transport and homeostasis by Rab11. *Mol. Biol. Cell* **13**, 3107–3122 (2002).
56. Tao, H. et al. Macrophage SR-BI modulates autophagy via VPS34 complex and PPAR alpha transcription of Tfeb in atherosclerosis. *J. Clin. Invest.* **131**, 16 (2021).
57. Lei, Q. et al. Deficient chaperone-mediated autophagy promotes inflammation and atherosclerosis. *Circ. Res.* **129**, 1141–1157 (2021).
58. Ma, L. et al. Ras-Raf-MAPK signaling promotes nuclear localization of FOXA transcription factor SGF1 via Ser91 phosphorylation. *Biochim. Biophys. Acta Mol. Cell Res.* **1865**, 560–571 (2018).
59. Tu, H. et al. Linear ubiquitination of RIPK1 on Lys612 regulates systemic inflammation via preventing cell death. *J. Immunol.* **207**, 602–612 (2021).
60. Ida, Y., Hikage, F. & Ohguro, H. ROCK inhibitors enhance the production of large lipid-enriched 3D organoids of 3T3-L1 cells. *Sci. Rep.* **11**, 5479 (2021).
61. Cui, M. et al. Involvement of cholesterol in hepatitis B virus X protein-induced abnormal lipid metabolism of hepatoma cells via up-regulating miR-205-targeted ACSL4. *Biochem. Biophys. Res. Commun.* **445**, 651–655 (2014).
62. Brown, R. J., Shao, F., Baldán, A., Albert, C. J. & Ford, D. A. Cholesterol efflux analyses using stable isotopes and mass spectrometry. *Anal. Biochem.* **433**, 56–64 (2013).

Acknowledgements

The authors acknowledge the Red Cross Society of Shandong Province in China for providing autopsy specimens and the Animal Care Centre of Qilu Hospital of Shandong University for their expertise. This work was supported by grants from the National Natural Science Foundation of China (No. 82270487 to M.Z., 82241203 to C.Z. and 82200502 to J.Z.), the Postdoctoral Science Foundation of China and Shandong Province (No. 2022M710084 to J.Z.), the Shandong Provincial Natural Science Foundation (ZR2023JQ030 to M.Z., 2021ZDSYS05 to M.Z. and ZR2022QH089 to J.Z.), the National Key Research and Development Program of China (2021YFF0501403 to C.Z.), Non-profit Central Research Institute Fund of Chinese Academy of Medical Sciences (2023-PT320-06 to M.Z.), the Taishan Scholars Program of Shandong Province (M.Z. and C.Z.) and the Fundamental Research Funds for the Central Universities (No. 2023QNTD003 to M.Z.).

Author contributions

C.Z., M.Z., and C.G. conceived and supervised the study. Y.Z. and B.X. assisted with the experimental design. Y.L., X.Z., L.Y., L.C. (Lei Cao), J.Z., and Q.L. performed experiments and analyzed data. X.W., W.Q., L.C. (Liangyu Cai), and R.R. assisted with experimental performance and data interpretation. W.W., X.G., and G.S. performed human sample analysis. Y.L. wrote the manuscript that was reviewed by all authors.

Competing interests

The authors declare no competing interests.

Additional information

Supplementary information The online version contains supplementary material available at https://doi.org/10.1038/s41467-025-57404-6.

Correspondence and requests for materials should be addressed to Chengjiang Gao, Meng Zhang or Cheng Zhang.

Peer review information *Nature Communications* thanks the anonymous reviewers for their contribution to the peer review of this work. A peer review file is available.